Rock Mech Rock Eng (2015) 48:1647–1671
DOI 10.1007/s00603-014-0656-z

ORIGINAL PAPER

Underground Excavation Behaviour of the Queenston Formation: Tunnel Back Analysis for Application to Shaft Damage Dimension Prediction

Matthew A. Perras · Helmut Wannenmacher · Mark S. Diederichs

Received: 23 June 2014 / Accepted: 19 September 2014 / Published online: 26 September 2014

Abstract The Niagara Tunnel Project (NTP) is a 10.1 km long water-diversion tunnel in Niagara Falls, Ontario, which was excavated by a 7.2 m radius tunnel boring machine. Approximately half the tunnel length was excavated through the Queenston Formation, which locally is a shale to mudstone. Typical overbreak depths ranged between 2 and 4 m with a maximum of 6 m observed. Three modelling approaches were used to back analyse the brittle failure process at the NTP: damage initiation and spalling limit, laminated anisotropy modelling, and ubiquitous joint approaches. Analyses were conducted for three tunnel chainages: 3 + 000, 3 + 250, and 3 + 500 m because the overbreak depth increased from 2 to 4 m. All approaches produced similar geometries to those measured. The laminated anisotropy modelling approach was able to produced chord closures closest to those measured, using a joint normal to shear stiffness ratio between 1 and 2. This understanding was applied to a shaft excavation model in the Queenston Formation at the proposed Deep Geological Repository (DGR) site for low and intermediate level nuclear waste storage in Canada. The maximum damage depth was 1.9 m; with an average of 1.0 m. Important differences are discussed between the tunnel and shaft orientation with respect to bedding. The models show that the observed normalized depth of failure at the NTP would over-predict the depth of damage expected in the Queenston Formation at the DGR.

M. A. Perras (✉) · M. S. Diederichs
Queen's University, Kingston, ON, Canada
e-mail: matthew.perras@erdw.ethz.ch

H. Wannenmacher
Marti AG, Bern, Switzerland

Keywords Underground excavations · Anisotropy · Spalling · Numerical modelling · Back analysis · Excavation damage

List of symbols

a_p	Peak Hoek–Brown material constant
a_r	Residual Hoek–Brown material constant
CI	Crack initiation
E	Intact rock modulus
E_{beam}	Beam modulus (material between joint elements)
Erm	Rock mass modulus
K_{Hh}	Maximum-to-minimum horizontal stress ratio
K_{hv}	Minimum horizontal-to-vertical stress ratio
K_N	Joint/lamination normal stiffness
K_o	Maximum horizontal-to-vertical stress ratio
K_S	Joint/lamination shear stiffness
m_p	Peak Hoek–Brown material constant
m_r	Residual Hoek–Brown material constant
p_0	Hydrostatic in situ stress
p_i	Internal support pressure
r	Maximum overbreak depth
R	Radius of the excavation
S	Joint/lamination spacing
s_p	Peak Hoek–Brown material constant
s_r	Residual Hoek–Brown material constant
T	Tensile strength
UCS	Unconfined compressive strength
u_{ie}	Elastic excavation convergence
σ_1	Maximum principal stress
σ_3	Minimum principal stress
σ_H	Maximum horizontal stress
σ_{max}	Maximum tangential stress at an excavation boundary
σ_v	Vertical stress
υ	Poisson's ratio

ϕ	Friction angle
ψ	Dilation angle

Abbreviations

AECL	Atomic Energy of Canada Ltd
BTS	Brazilian tensile strength
DGR	Deep geological repository
DISL	Damage initiation and spalling limit
DTS	Direct tensile strength
EDZi	Inner excavation damage zone
EDZo	Outer excavation damage zone
GSI	Geological strength index
HDZ	Highly damaged zone
LAM	Laminated Anisotropy Modelling
NTP	Niagara tunnel project
NWMO	Nuclear Waste Management Organization of Canada
SAB	Sir Adam Beck generating station
TBM	Tunnel boring machine
UBJT DY	Ubiquitous joint double yield

1 Introduction

The Queenston Formation is an extensive sedimentary layer in both the Appalachian and Michigan sedimentary basins of North America. It is exposed at the surface along the base of the Niagara Escarpment, as shown in Fig. 1. It is an important raw material for the brick industry, and many civil engineering projects have been constructed on or in the Queenston rock mass. The most recently completed, the Niagara Tunnel Project (NTP), is a 7.2 m radius water diversion tunnel in the city of Niagara Falls, Ontario, Canada. Of the total 10 + 200 m length of the tunnel, approximately 5 + 000 m were excavated within the Queenston Formation. The tunnel gradient was shallow relative to the bedding dip throughout most of the tunnel.

In contrast, a shaft excavation perpendicular to the bedding is being proposed for access to and ventilation of a Deep Geological Repository (DGR) for Low and Intermediate Level Nuclear Waste storage in the Cobourg Formation. Extensive investigations have been conducted at the Bruce Nuclear Power Station for this DGR, where the Queenston Formation is approximately 73 m thick. These two projects are used to study the effect of the excavation orientation on the rock mass behaviour and to determine the influence of anisotropy on the damage zone dimensions.

1.1 The Niagara Tunnel Project

The NTP is a water diversion tunnel for hydropower generation. The tunnel diverts water from above Niagara Falls to the Sir Adam Beck (SAB) generating station, as shown in Fig. 2a. The project decreased the amount of time that

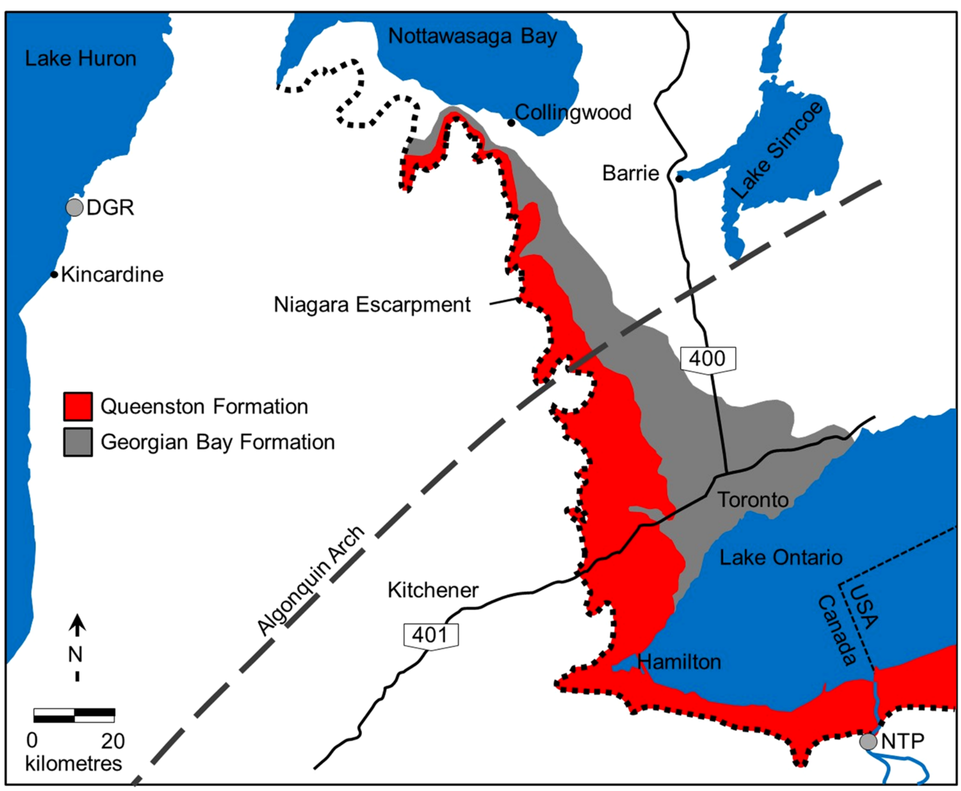

Fig. 1 Regional surface exposure of the Queenston and Georgian Bay Formations in Southern Ontario showing the NTP and DGR site locations (modified from Armstrong and Carter (2010) and Russell (1981))

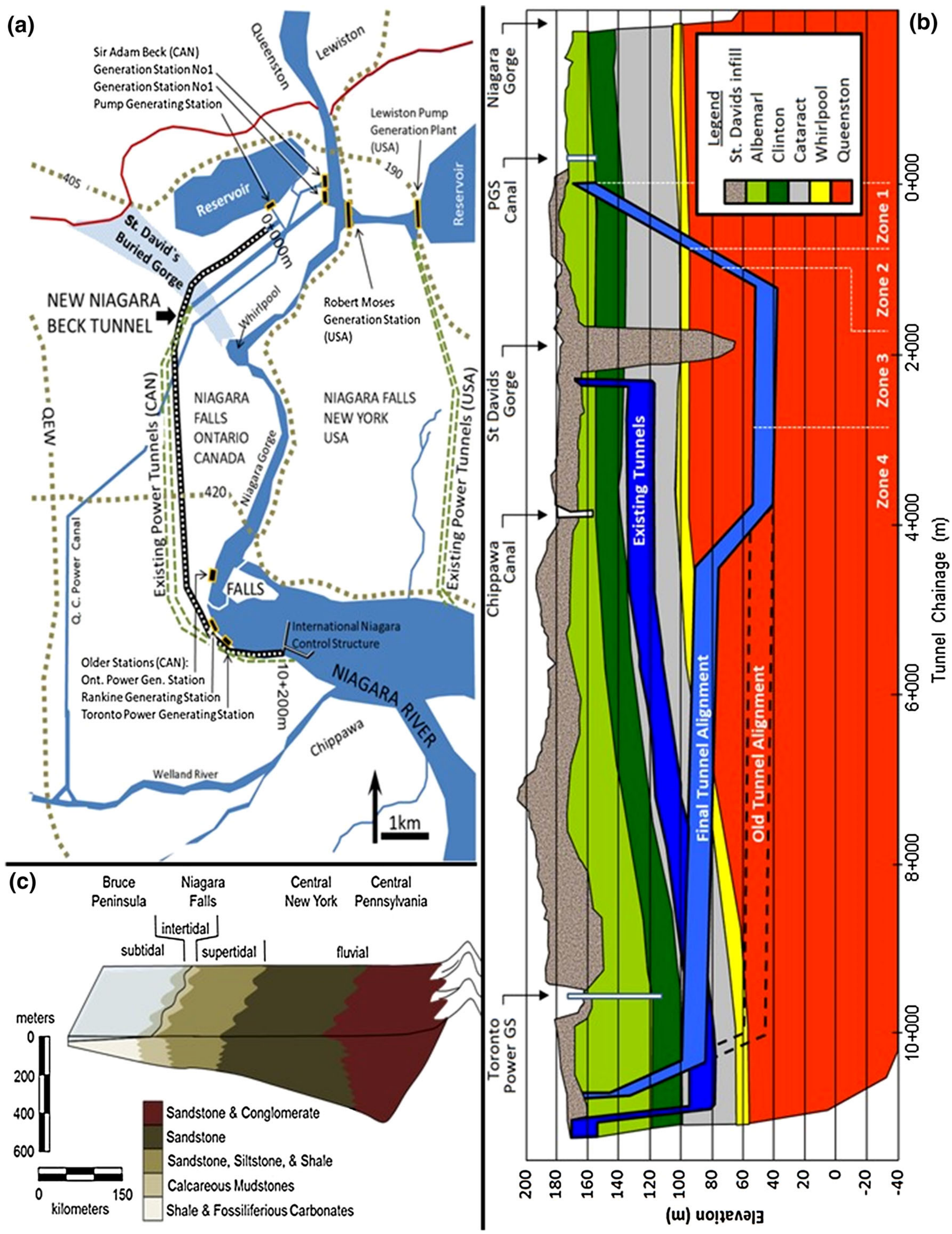

Fig. 2 An overview of the Niagara Tunnel Project showing **a** the plane view of the tunnel in relation to existing infrastructure, **b** a longitudinal cross section along the tunnel alignment showing the main geological units (modified from Perras et al. 2014), and **c** the depositional setting of the Queenston (after Brogly et al. 1998)

the available water for diversion exceeds the SAB capacity from 65 to 15 % (Delmar et al. 2006). Excavation of the NTP began in August 2006 and was completed in May 2011. The project went into operation in March 2013.

The tunnel was excavated using an open gripper tunnel boring machine (TBM), which required modifications during construction to meet the challenging geological conditions (Gschnitzer and Goliasch 2009). The overbreak was focused in the crown and invert as a result of the high horizontal stress ratio. The bedding reportedly dips 4 m/km (Novakowski and Lapcevic 1988) and can be considered nearly horizontal at the scale of the tunnel. The overbreak in the section of the tunnel within the Queenston Formation typically reached 4 m in the high stress areas, with local maximums reaching 6 m, and presented significant tunnelling difficulties. Observations of the excavation performance were documented by Perras et al. (2014), up to chainage 3 + 500 m.

The nearly horizontal tunnel alignment, in the Queenston Formation (see Fig. 2b), closely parallels the bedding and this orientation contributed to the overbreak (Perras et al. 2014). The deposition of the clastic material started in the south-east and moved in a north-westerly direction and as a result the Queenston became finer grained in this direction. Fluctuating sea levels would cause local variations also. The variations in the grain size has a direct influence on the strength and stiffness of the intact rock samples, which will be discussed later in the paper. These variations, as well as variations in the stresses, contributed to changes in the overbreak geometry, as documented by Perras et al. (2014).

The behaviour of the Queenston Formation from the NTP presents an opportunity to back analyse the deformations to determine the appropriate strength, stress, and anisotropic properties that give rise to numerical results similar to those measured in the tunnel (see Perras et al. 2014). This understanding is then applied to the DGR shaft excavation in the Queenston Formation for forward prediction.

1.2 The Deep Geological Repository

The Nuclear Waste Management Organization (NWMO) is proposing to construct a DGR approximately 250 km northwest of the NTP. The proposed site is located below the site of the Bruce Nuclear Generating Station. The footprint is shown in Fig. 3a in relation to the reactor buildings (Bruce A and Bruce B), and emplacement horizon is proposed to be in the Cobourg Formation (Fig. 3b), at approximately 680 m below the ground surface. The project will include an access shaft with a radius of approximately 4 m and a slightly smaller ventilation shaft. A 200-m-thick shale sequence, including the Queenston Formation, overlies the Cobourg and forms a regional aquitard. The shale formations provide a natural barrier between saline basin fluids and the overlying ground water resources near the ground surface.

As part of the regulatory approval process for the DGR, the Environmental Impact Statement, Preliminary Safety Report, and other supporting documents were submitted to the Canadian Nuclear Safety Commission Review Panel on April 14, 2011. For a detailed review of the project and the geological setting, the reader is referred to the Descriptive Geosphere Site Model (Intera Engineering Ltd 2011) and the Geosynthesis (NWMO 2011) reports.

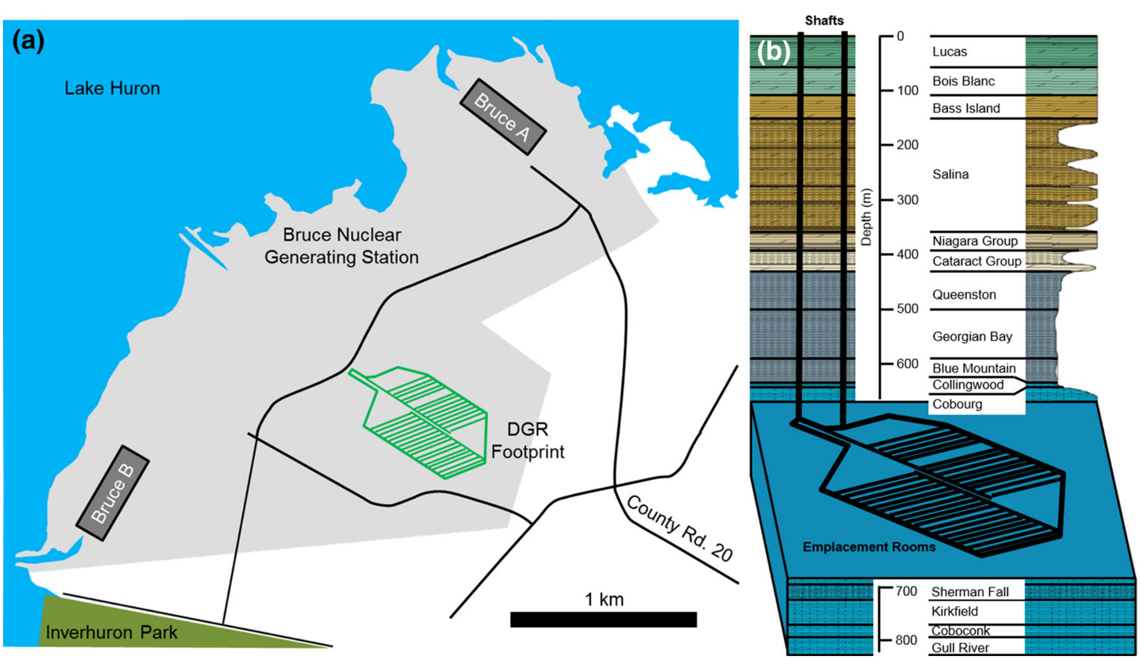

Fig. 3 Overview of the Bruce Nuclear site on the eastern coast of Lake Huron showing the location of **a** the DGR footprint in relation to the Bruce Nuclear site and the reactors (Bruce A and Bruce B) and **b** the geological stratigraphy (modified from NWMO 2011) with the emplacement horizon in the Cobourg at an elevation of 680 m below ground

This paper investigates issues related to the back analysis of the NTP, with the goal of understanding the 5 key numerical inputs that reliably reflect the observed overbreak. Taking these findings, and accounting for site specific variations, numerical modelling is presented to assess the behaviour of the Queenston during simulated shaft excavation.

2 Geological Setting

The NTP is located in the Appalachian sedimentary basin, and the DGR is located in the Michigan sedimentary basin (Fig. 1). The Appalachian basin is a back arc basin, and the Michigan basin is an inner cratonic basin. This means that there are more coarse-grained sedimentary rocks and higher stresses in the Appalachian basin because of closer proximity to the fold and thrust belts of eastern Canada and the USA than in the Michigan basin. The Michigan basin has more carbonate and evaporite deposits because of periods of isolation from the ocean which is typical of inner cratonic basins (Sloss 1953). The isolation was caused by the Algonquin Arch, which is a high ridge in the Precambrian basement rock. Some sedimentary formations are truncated forming unconformities across the arch, which suggests that intermittent uplift was occurring during deposition of the sediments in both basins (Stearn et al. 1979).

The sedimentary rocks of Southern Ontario, within the basins, range from Cambrian to Devonian, with the younger formations outcropping at the surface in southwestern Ontario. The sediments were derived from the Taconic Mountains (Fig. 2c). The Queenston and Georgian Bay formations were deposited during the Upper Ordovician. The Queenston Formation gradationally overlies the Georgian Bay Formation.

2.1 Regional Character

The Queenston Formation outcrops along the base of the Niagara Escarpment, which runs from northern New York State, along the western shore of Lake Ontario and up to the tip of the Bruce Peninsula, where it continues below the water of Lake Huron (see Fig. 1). The Formation lies over the shales and interbedded limestones of the Georgian Bay Formation and is separated at its upper boundary by an unconformity with the Whirlpool sandstone, in Niagara Falls, Ontario. The Whirlpool gradually grades into dolostones of the Manitoulin Formation (Winder and Sanford 1972). Bergstrom et al. (2011) suggest that the Whirlpool disappears northwest of the Algonquin arch within the Michigan Basin.

On the regional scale, the Queenston Formation can include sandstone and conglomerate near the erosional source on the east coast of North America to fossiliferous carbonates near Lake Huron (Tamulonis and Jordan 2009). Brogly et al. (1998) stated that the Queenston was deposited in a subtidal to supertidal depositional environment in Ontario, which changed to a fluvial-dominated environment in central New York and Pennsylvania (see Fig. 2c). The Queenston Formation in Southern Ontario is predominately a calcareous mudstone to red shale and can contain interbeds of siltstone and limestone.

The thickness of the Queenston Formation decreases in a north-westerly direction, from greater than 300 m at the NTP site to 73 m at the DGR site (Sandford 1961). As the Queenston thins, it grades into the upper part of the Georgian Bay Formation (Armstrong and Carter 2006). The regional variations in the depositional environment influence the site-specific strength, stiffness, and stress levels differently. However, similarities still exist despite the distance between the two sites.

2.2 Site Comparison

To numerically back analyse the NTP and evaluate the potential degree of excavation damage at the DGR, the site specific properties are compared to determine if they are within suitable ranges to make similar numerical methods applicable. To compare the laboratory testing results on intact Queenston core samples, the depth datum has been taken as the top of the Queenston Formation for each site. This is an imperfect datum as the Queenston thickness varies considerably between the two sites. However, it does give a frame of reference for comparison and should account for the effects of regional changes in deposition on the properties. Greater local variations in deposition may account for the differences in the strength and stiffness trends between the two sites, discussed in the following sections.

2.2.1 Numerical Model Inputs

The Unconfined Compressive Strength (UCS), Crack Damage (CD) and Crack Initiation (CI) values are important input parameters for brittle modelling, as defined by Diederichs and Martin (2010) according to the constitutive model of Diederichs (2007) and illustrated in Fig. 4.

For hard, brittle rocks such as granite, it is well known that the in situ strength drops from the yield threshold (CD) to a lower bound value (CI) determined during laboratory testing (Diederichs 2003).The reason for this drop is particularly sensitive to confinement such that as the confining stress increases, the ability for cracks to propagate (reach CD) once initiated (at CI) becomes limited. Away from an excavation for example, it is possible to have micro-crack damage with no visible or significant mechanical influence,

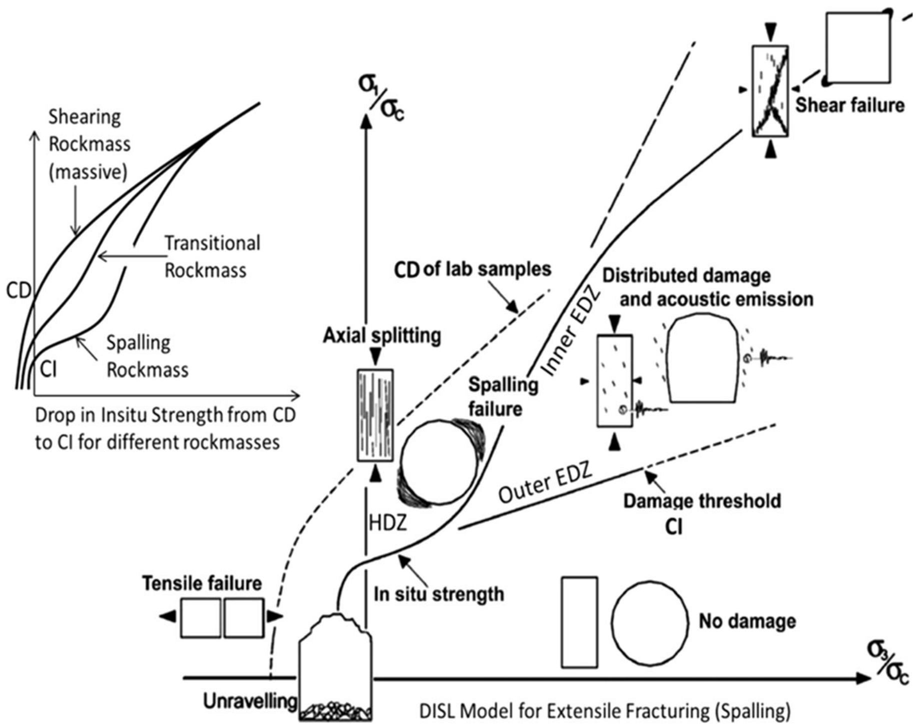

Fig. 4 DISL spalling conceptual model (Diederichs 2007) with inset showing the transition from lab testing CD threshold, for yield, to lower bound CI for spalling rocks. Other rocks yield in shear or show a combination (transitional) behaviour (modified from Perras et al. 2013)

such as in the outer Excavation Damage Zone or EDZo. Closer to the excavation surface, cracks are less confined and more capable of propagating and connecting, which reduces the stiffness and ultimate strength of the material and increases the rock mass permeability. Near excavation fractures, once initiated, propagate spontaneously such that the observed wall strength of the excavation drops to the lower bound CI value. This model is applicable to crystalline rocks and is labelled as the 'spalling rock mass' curve in the inset of Fig. 4. Martin (1997) and Diederichs (2007) demonstrated that a good correlation between observed depth of spalling and the stress to strength ratio exists for brittle rocks. Martin (1997) correlated these observations to UCS and Diederichs (2007) to CI.

Other rock types such as mudstones and siltstones do not necessarily follow this model. Cracks may not spontaneously propagate as they do in hard rocks such as granites. Thus, damage may not develop into observable or significant mechanical damage as is observed in the inner Excavation Damage Zone (EDZi) or the Highly Damaged Zone (HDZ).

These rocks typically behave as a 'shearing rock mass', as shown in the inset of Fig. 4 (upper left). If, however, the plane of weakness (bedding plane) is parallel to the orientation of the most likely extension crack propagation direction, then the damage that begins at CI will migrate to these bedding planes and exploit them for propagation and ultimate failure. This behaviour can be considered transitional between shearing and spalling. In any case, the thresholds for CD and CI are important mechanical parameters for damage and failure prediction.

2.2.2 *Mechanical Properties of the Queenston*

Extensive testing for both projects has been carried out, including unconfined, triaxial, and tensile tests. These are the fundamental tests required to describe the failure envelope of the intact rock and the rock mass. The NTP testing was conducted at various laboratories over an extended period of time during the investigation stage of the project (the mid-1980s to 1998). During this time frame, it was established that brittle rock mass failure around excavations often occurred when the stress concentration exceeded 30–60 % of the peak laboratory strength, or the CI threshold (Martin 1997, Read et al. 1998). However, the importance of CI as an input parameter for numerical brittle spall prediction was not yet widely accepted in practice during the design of the NTP and its application was generally limited to high strength crystalline rocks until observations at the NTP suggested that the failure mechanism was a brittle process (Perras et al. 2014).

Although numerous UCS tests were conducted, as shown in Fig. 5a, only a limited number of the completed tests included volumetric strain measurements, which can be used to determine CD and CI. The volumetric strain reversal point and the onset of the non-linearity of lateral strain points were used to determine the CD and CI thresholds, respectively, based on the test data from the

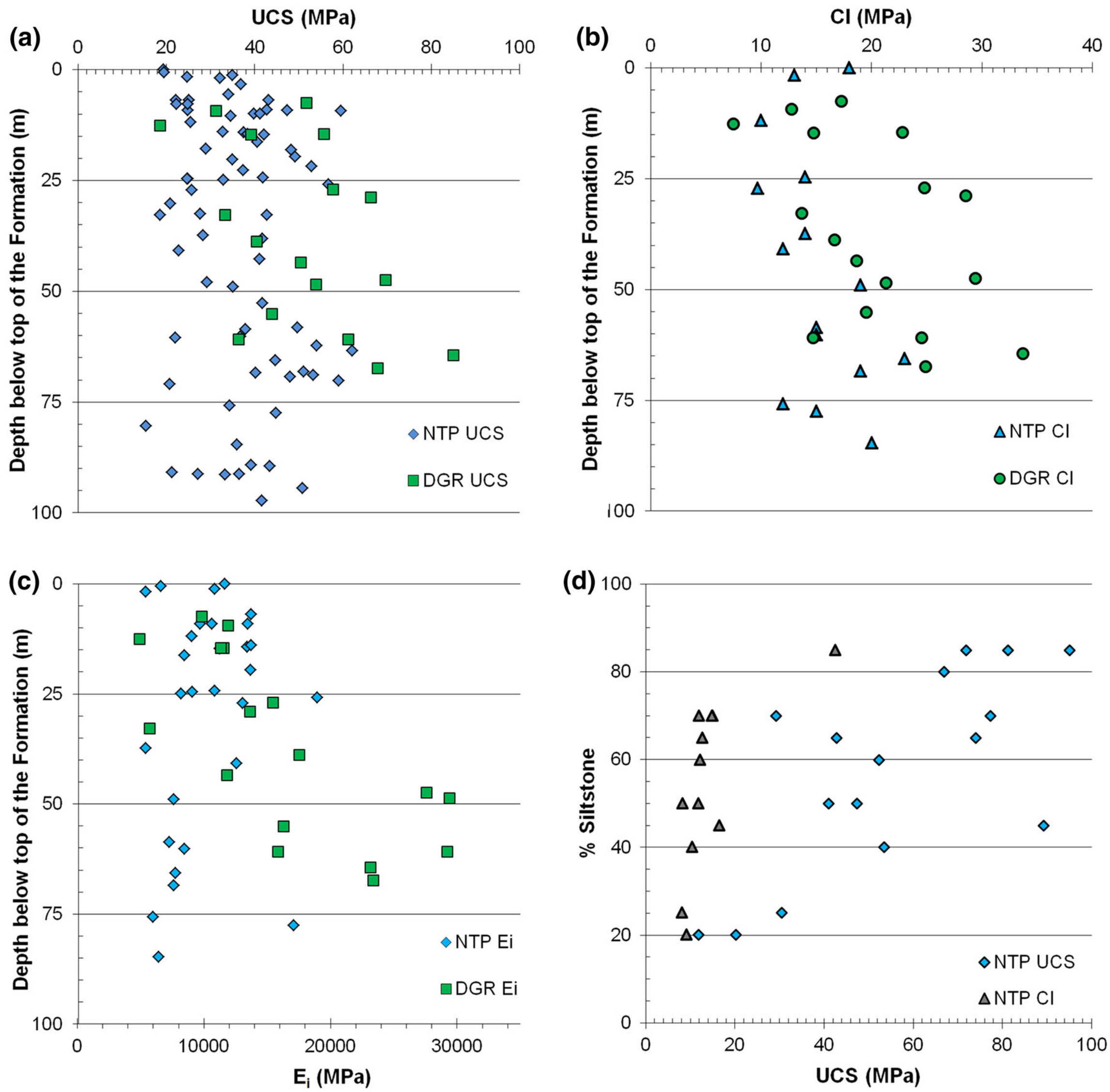

Fig. 5 Comparison of **a** UCS, **b** CI, and **c** Young's Modulus, E_i, between the NTP and the DGR of the Queenston Formation. Influence of the siltstone content is shown in (**d**). Data courtesy of Ontario Power Generation

NTP (courtesy of Ontario Power Generation). The values for the DGR were taken directly from various testing reports (Gorski et al. 2009, 2010, 2011). The reader is referred to Ghazvinian et al. (2013) for details on the methods for determining CD and CI. For clarity, only UCS and CI are plotted in Fig. 5, with respect to the depth datum and percentage of siltstone content. The test results are also summarized in Table 1.

The strength values in Fig. 5 have been plotted using the top of the Queenston Formation as the datum. At first inspection, it seems that there is a wide range of strength values for both the NTP and DGR. In fact, Fig. 5a indicates a wider range at the DGR site. The DGR UCS and CI values increase with depth (Fig. 5a, b).

Table 1 Summary of properties for the Queenston Formation at the NTP site (raw stress–strain data courtesy of Ontario Power Generation) and the DGR site as reported in Gorski et al. (2009, 2010, 2011)

	CI (MPa)	CD (MPa)	UCS (MPa)	T (MPa)	m_i	E_i (GPa)	ν
NTP							
Avg.	15.3	27.5	39.0	2.48	11	11.3	0.36
Min.	8.1	14.9	15.4	1.09	5	5.4	0.18
Max.	42.4	112.1	112.9	4.29	14	32.2	0.49
DGR							
Avg.	22.2	36.8	52.8	–	–	17.4	0.32
Min.	7.6	15.1	18.8	–	–	5.0	0.10
Max.	33.8	75.4	85.5	–	–	34.4	0.44

This could be partially related to the transition to the Georgian Bay Formation, at the base of the Queenston, which contains more siltstone and limestone interbeds. This would also account for the increasing stiffness with depth at the DGR site (Fig. 5c), although siltstone content was not measured for samples at the DGR, this has been inferred from measurements from the NTP. Examining the UCS values with respect to the siltstone percentage shows that the UCS generally increases with increasing siltstone content, whereas the CI value is largely unaffected below 80 % (Fig. 5d).

Amann et al. (2011) investigated crack initiation in the Opalinus clayshale and indicated that tensile cracks began in the stiffer layers, and shear cracks began in the softer layers as a result of the stiffness contrast. In the case of the Queenston, the siltstone layers are stiffer and, according to Amann et al. (2011), should be where cracks first occur. Because CI has been determined as the point where the lateral strain deviates from linearity, the data suggest that the lateral strain deviation is controlled by the presence of the siltstone, irrespective of the percentage (up to 80 %). The lateral stiffness is controlled by the shale layers (even at higher siltstone content), and because the stiffness of the siltstone is incompatible with the shale, tensile cracks develop in the siltstone. Above 80 % siltstone, a sample's lateral stiffness must switch to being controlled by the siltstone, which is stronger. The result is a high CI. The siltstone layers absorb cracks during loading, which cannot propagate further through the shale layers. This influences the peak strength. With increasing siltstone, this peak strength also increases because there is a greater volume for crack absorption in the sample during loading. The layering also gives rise to anisotropic strength and stiffness, but does not influence CI, as mentioned previously.

The thickness of the Queenston Formation is over 300 m at the NTP site, and only the upper portion was investigated for the numerical back analysis, within the tunnel horizon. The UCS values in the upper portion of the Queenston Formation at the NTP site show a wide range, which is generally consistent with the depth. A closer examination indicates that there are potentially three strength bands, which all exhibit increasing strength with depth. The first band is at 0–25 m, whereas the second and third have depth ranges of 25–75 and 75–100 m, respectively. Similar bands can be seen in the CI thresholds. These bands are likely related to changes in the depositional environment.

The carbonate content of the Queenston, including disseminated crystals in the shale matrix and interbeds of limestone, which increases to the northwest away from the Taconic source zone, and it has been reported that the lower part of the Queenston consists of thinly interbedded and interlaminated siltstone, sandstone, and limestone, with red and green shale (Armstrong and Carter 2006). Thus, the increasing strength and stiffness with depth and distance from the source could be associated with the increase in the calcite content, similar to an increase in slake durability with increasing calcite content found by Russell (1981).

The Direct Tensile Strength (DTS) was only measured on a limited number of samples for the NTP. The average DTS was determined to be 1.45 MPa for samples tested perpendicular to the bedding. This value can be considered to be the tensile strength of the bedding planes within the Queenston Formation at the NTP. The minimum DTS is reported in Table 1. Brazilian tensile strength (BTS) testing was more commonly completed for the NTP, and the average BTS, 4.29 MPa, was used as the maximum tensile strength because it has been determined that BTS is typically 30 % higher than the equivalent DTS for sedimentary rocks (Perras and Diederichs 2014). The same tensile values were used for the DGR models.

The minimum and maximum values are reported in Table 1. For both the NTP and DGR, three groups of properties were used as input for the numerical models. The minimum and maximum values, reported in Table 1, were considered to represent the range of values over six standard deviations. These were used to determine plus or minus one standard deviation and, along with the average values, these three groupings of properties (Table 2) were used in the numerical models to understand the influence on the overbreak dimensions.

2.2.3 Stress Conditions

Throughout southern Ontario, high residual in situ horizontal stresses exist in the sedimentary rocks, which were locked in as a result of tectonic activity during the Appalachian mountain building events, sedimentary basin effects and glacial loading and erosion. Stress shadows can occur at formation boundaries as a result of differences in the elastic properties (Haimson 1983; Gross et al. 1995).

At the NTP, the deepest section of the tunnel, in the Queenston, is 140 m below the ground surface. For the

Table 2 Specific strength and stiffness values for the NTP (Perras et al. 2014) and for the DGR shaft (Gorski et al. 2009, 2010, 2011) used in the numerical modelling

	CI (MPa)	CD (MPa)	UCS (MPa)	T (MPa)	E_i (GPa)
NTP					
+1 Sd Dev.	17.5	31.8	49.1	3.0	15.8
Mean	15.3	29.8	44.7	2.5	11.3
−1 Sd Dev.	13.0	27.8	40.3	2.0	6.8
DGR					
+1 Sd Dev.	24.8	46.8	64.0	3.0	22.3
Mean	20.4	36.8	52.8	2.5	17.4
−1 Sd Dev.	16.0	26.7	41.7	2.0	12.5

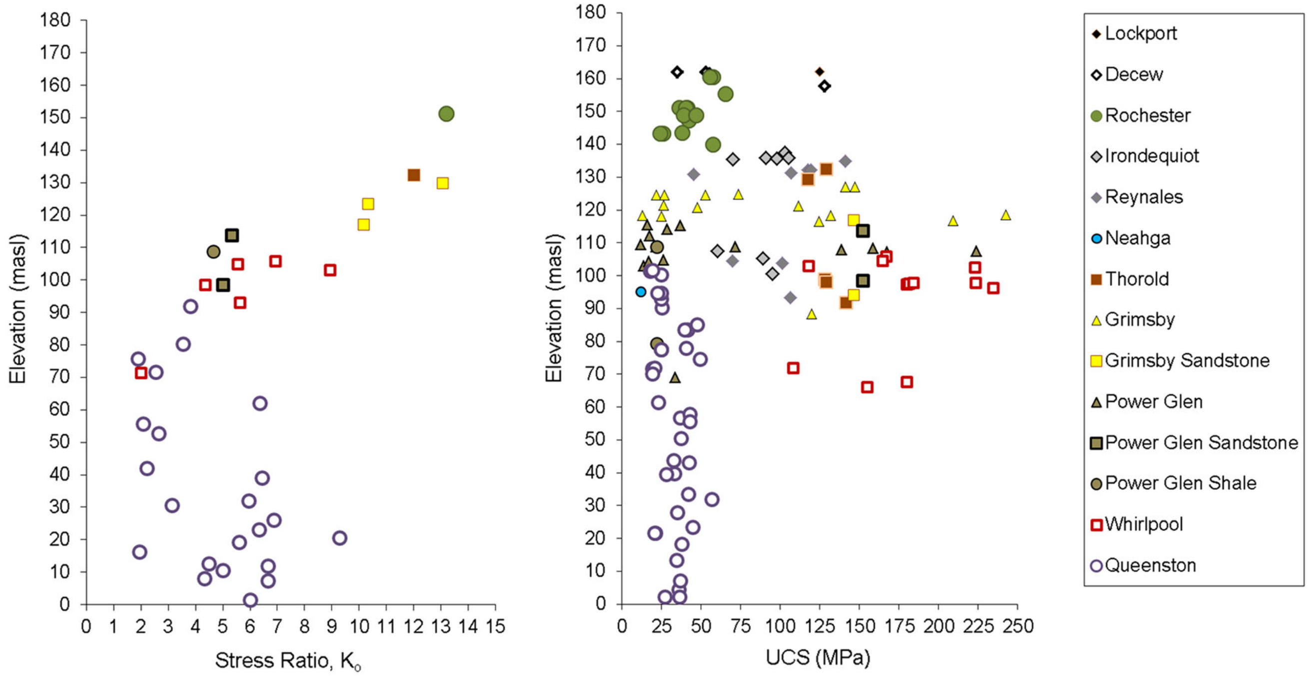

Fig. 6 Stress ratio measurements from the NTP for **a** the vertical stress ratio, K_o, and **b** the horizontal stress ratio, K_{Hh}

purposes of the modelling in this paper, the vertical stress has been assumed to be the weight of the overlying rock mass. Perras et al. (2014) showed that there is a stress magnitude discontinuity at approximately 6 m below the deepest section of the tunnel. This results in a wide maximum horizontal-to-vertical stress ratio (K_o) range of 2–9, and a horizontal stress ratio (K_{Hh}) range of 1–2.5 in the Queenston Formation, as shown in Fig. 6. The typical K_o at the elevation of the tunnel (140 m below the ground surface) ranges between 2 and 6. The wide range of potential stresses has been used to determine the variations in the numerical predictions of the depth of yielding in comparison to measurements from the NTP. Stresses at the DGR site have been estimated using a variety of methods (Intera Engineering Ltd. 2011; NWMO 2011). The K_o ratio has a range of 0.5–1.6; K_{Hh} has a range of 1.0–3.2; and the minimum horizontal-to-vertical stress ratio (K_{hv}) has a range of 0.5–1.2 (NWMO 2011).

3 Overbreak at the NTP

Observations up to chainage 3 + 500 m of the tunnel were documented by Perras et al. (2014) who defined four zones of behaviour (Fig. 2b), three of which are within the Queenston. Zone 1 is defined as all the formations above the Queenston. Zone 2 is at the contact area between the Whirlpool and Queenston formations, which is a disconformity. The reduction in stress due to a stress shadow, and jointing, created conditions permitting large blocks to fall from the crown. The overbreak was observed to break back to the overlying Whirlpool Formation to a maximum depth of 1.4 m, at which time forward spiling support was used to advance the tunnel. When the tunnel reached its maximum depth (140 m), stress-induced failure was observed. However, the behaviour was influenced by St. Davids Buried Gorge, which the tunnel had to pass under.

On reaching the structural influence of the buried gorge (Zone 3), the overbreak was on the order of 2.0 m, as shown in Fig. 7. It should be noted that through most of this zone, forepoles were used to stabilize the ground ahead of the excavation. Vertical jointing, spaced 2–3 m, and horizontal and inclined shear surfaces were observed. The joints remained clamped as a result of the stress concentration and had a minor influence on the overbreak geometry. The shear surfaces likely affected the overbreak depth, although this was not directly observed. The overbreak geometry remained asymmetric throughout this zone. However, it was generally inconsistent in size and shape because of the irregular depth to the bottom of St. Davids Buried Gorge.

Stress-induced fracturing became more prominent as the tunnel moved away from the influence of the buried gorge, marking the transition to stress-induced overbreak in Zone 4. The crown overbreak formed an arch 7–8 m wide with a consistent notch shape, skewed to the left as shown in Fig. 8, which likely indicates a high stress ratio with the major principal stress orientation slightly inclined from the

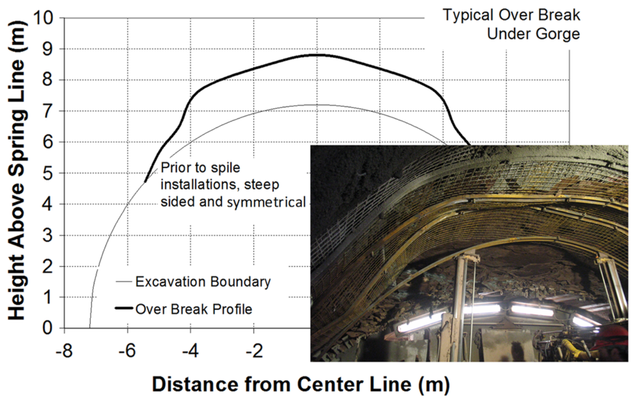

Fig. 7 Typical overbreak profile in Zone 3 under St. Davids Buried Gorge, prior to spile installation, with *inset* photo (from Perras 2009)

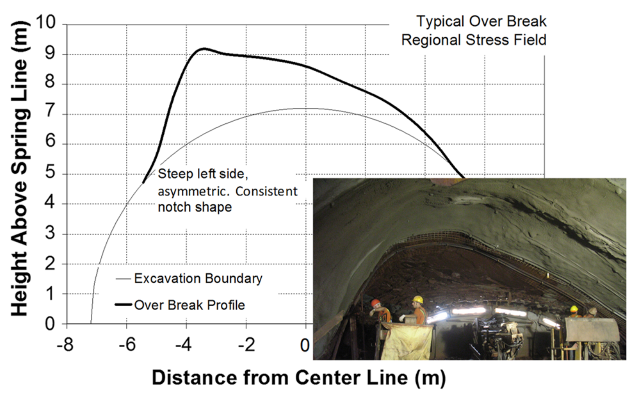

Fig. 8 Typical overbreak profile for the high horizontal stress field in overbreak Zone 4. *Inset photo* showing overbreak up to $\sim$3 m deep (from Perras 2009)

horizontal. The overbreak reached a maximum depth of 6 m. However, it was more typically in the range of 3–4 m deep.

Failure in the invert continued with induced spall planes, which were marked with plumose and conchoidal surfaces. Although minor sidewall spalling occasionally occurred in the sidewall area, it was limited to vary shallow surficial damage when it occurred.

Detailed measurements of the crown maximum overbreak, apex angle of the overbreak notch, and chord closure were presented by Perras et al. (2014), up to a chainage of 3 + 500 m within the tunnel. The maximum, mean, and minimum overbreak depth and chord closure measurements between tunnel chainages of 3 + 000 and 3 + 500 m have been used for the back analysis. Over these chainages there was a large increase in both overbreak depth and chord closure.

The section used for the back analysis is the transition from the influence zone of St. Davids Buried Gorge (Zone 3) into the higher stress field influence (Zone 4). The numerical modelling has focused on the crown measurements to determine the strength and stress conditions that give rise to similar numerical results. With an understanding of the appropriate modelling method, the input properties that gave reasonable results similar to the observations at NTP have been used for forward numerical prediction at the DGR.

4 Numerical Models

The notch at the NTP in the Queenston Formation formed through brittle failure, as observed by the authors. The brittle failure process can be captured numerically using the Damage Initiation and Spalling Limit (DISL) approach of Diederichs (2007). Work by several authors (e.g. Perras (2009); Barla et al. (2011); Fortsakis et al. (2012)) has demonstrated that when the anisotropic stiffness is captured in a numerical model using joint elements or other methods, the observed overbreak geometry and deformation pattern can be correctly simulated. These approaches were implemented in the finite difference program Phase 2, by RocScience, as a preliminary assessment to determine the appropriate stress and rock mass properties for more advanced analysis. To capture the influence of horizontal laminations on a vertical shaft, three-dimensional numerical models are necessary. Advanced analyses have been conducted using the finite difference program FLAC 3D, by Itasca, to capture the lamination influence on the rock mass behaviour. This has been done using the ubiquitous joint double yield (UBJT DY) model in FLAC 3D (Itasca 2009). The modelling methods will be discussed in more detail below.

4.1 Failure Criteria

Brittle failure is the result of extensile fractures forming parallel to the excavation surface under compressive loading. A focal point of stress creates localized damage, which then concentrates the stress around the local damage. This in turn creates more localized damage. In this manner, the damage is localized into a notch geometry, which is typical for brittle failure around underground excavations (Martin 1997).

Several numerical approaches have been used to capture the brittle behaviour process (Martin 1997; Hajiabdolmajid et al. 2002; Diederichs 2007). Diederichs (2007) developed a method to represent brittle behaviour using the generalized Hoek–Brown (Hoek et al. 2002) peak and residual parameters, which are standard input parameters for engineering design software. The DISL method of Diederichs (2007) requires CI, the UCS thresholds, and the tensile

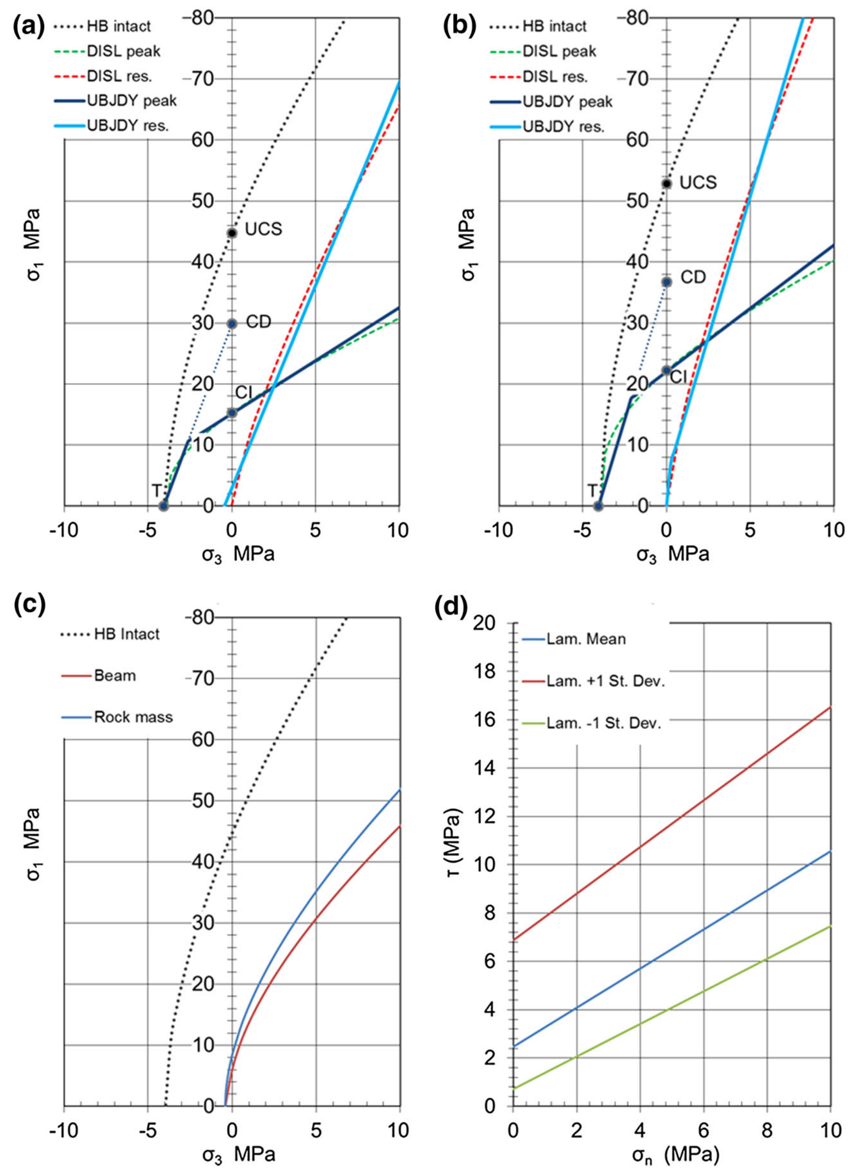

Fig. 9 The failure envelopes for: **a** the NTP—DISL and UBJT DY models, **b** the DGR—DISL and UBJT DY models, **c** the NTP—the laminated (LAM) models, and **d** the lamination Mohr–Coulomb envelopes

strength as input properties. Rocks with UCS/T >9 and rock masses with GSI >55 can behave in a brittle manner [please note the specific limits in Diederichs (2007)]. Using the generalized Hoek–Brown (Hoek et al. 2002) parameters the peak and residual failure curves can be determined, using Eqs. 1 and 2, after Diederichs (2007):

$$s_p = \left(\frac{\mathrm{CI}}{\mathrm{UCS}}\right)^{\left(\frac{1}{a_p}\right)} \tag{1}$$

$$m_p = s_p\left(\frac{\mathrm{UCS}}{|T|}\right) \tag{2}$$

where a_p is a curve fitting parameter for the peak curve, taken as 0.25 in this paper. Diederichs (2007) suggested that the residual parameters, a_r, and s_r, should be 0.75 and 0.001, respectively. The residual parameter m_r should be between six and ten, and six was used in this paper for the DISL approach. The mean peak and residual DISL failure envelopes for the NTP and DGR are shown in Fig. 9a and b, respectively.

The Queenston Formation has anisotropic stiffness and strength (Lo and Lee 1990; Ghazvinian et al. 2013). Perras (2009) demonstrated that the anisotropic behaviour could be simulated using joint elements to capture the anisotropic stiffness of the rock mass. To ensure compatibility between the laminated area (with joints) and the non-laminated area, a relationship for the transversely isotropic elasticity was used to scale the modulus, which accounted for the normal stiffness (K_N) and spacing of the laminations (S) (see Eq. 3). Using these parameters and the beam modulus (in this case the intact modulus), E_{beam}, a non-laminated rock mass modulus, E_{rm}, can be equated using Eq. 3, as shown below (Brady and Brown 2006).

$$\frac{1}{E_{rm}} = \frac{1}{E_{beam}} + \frac{1}{K_N S} \quad (3)$$

The rock mass (without laminations) and the rock beams (in between laminations) have been modelled as a perfectly plastic Hoek–Brown (Hoek et al. 2002) material. The Hoek–Brown (Hoek et al. 2002) parameters, m_b and s, were also scaled, such that the rock mass properties (without joint elements) were compatible with the rock beams. This was done first by adjusting the GSI value, such that the modulus was the same as that calculated using Eq. 3, and then taking the m_b and s values and harmonically averaging these with the beam m_b and s values, following the methodology of Perras (2009). The intact, rock mass, and beam failure envelopes are shown in Fig. 9c.

The laminations (joint elements) provide a surface for lateral slip and detachment during convergence and deflection, respectively, which is not accounted for when using isotropic models such as the DISL approach. By modelling horizontal laminations with joint elements, the rock mass behaviour is controlled by both the beams and the laminations themselves.

The laminations reduce the rock mass modulus in the vertical direction and allow for greater joint parallel displacements over an equivalent isotropic numerical representation of a rock mass (Perras 2009). The laminations also allow for deflection of the rock beams into the excavation. This approach is called the Laminated Anisotropy Modelling Method (LAM) throughout the rest of this paper. The increases in the joint parallel displacement and beam deflection create a different deformed excavation boundary surface for the LAM model compared to the equivalent isotropic model. In the modelling presented in this paper, three different joint element Mohr–Coulomb failure envelopes were used to define the lamination properties, as shown in Fig. 9d. Perras (2009) showed that this numerical approach creates a plastic yield zone similar to that observed at the NTP.

The UBJT DY model allows for two Mohr–Coulomb segments to be used to define the failure envelope, as well as a tension cut-off. This model was chosen because of the simplicity of the input parameters, which only require cohesion, friction, and tensile cut-off values. Residual properties are activated by plastic strain levels over user-defined stages and do not require other plastic indicators to control the transition to residual properties, such as are required for the implementation of the DISL approach with the generalized Hoek–Brown (Hoek et al. 2002) failure criterion in FLAC3D (Itasca 2009). The model can consider a weaker plane of anisotropy. For this study, three different property sets were evaluated (Fig. 9d; Table 2).

The brittle rock mass properties were implemented in the UBJT DY model by selecting envelopes that approximate the DISL peak and residual envelopes. This was done by projecting the first segment of the yield surface from the tensile strength (T) to CD (see Fig. 9a, b). This appears to adequately capture the curvature of the DISL peak yield surface for both the NTP and the DGR. The second segment of the peak UBJT DY yield surface is fit between CI and the intersection of the DISL peak and residual envelopes. The residual DISL curve is approximated manually using a tensile strength close to zero.

The UBJT DY model allows for peak and residual properties to be captured using a strain softening/hardening approach, by utilizing the plastic shear strain as an indicator of when to decrease/increase the property. The properties used in the numerical modelling are summarized in Table 2. The plastic shear strain increments used to control the transition from the peak to residual in the FLAC3D models were determined following the work of Hajiabdolmajid (2001).

4.2 Geometry

For the NTP models, a back analysis was first conducted in two dimensions to determine the ranges of the strength and stress values that capture the observed overbreak geometry, as shown in Figs. 7 and 8. Two-dimensional cross sections were modelled at tunnel chainages of 3 + 000, 3 + 250, and 3 + 500 m, which corresponded to tunnel invert elevations of 46, 47, and 61 m, respectively. Three-dimensional models were also used to make a comparison with the LAM approach.

An outer numerical boundary radius of 70 m (5 × the tunnel diameter and consisted of a radial mesh geometry. The curved outer boundary was fixed in both the vertical and horizontal directions, and in the three-dimensional case, the model can move out of the plane, parallel to the tunnel orientation, with the ends of the models fixed. For the NTP models, the interior region near the excavation surface has zones with lengths of 0.16 and 0.5 m for the two- (DISL) and three-dimensional models, respectively. The LAM models capture the true stratigraphy of the NTP because of the close proximity of the contact between the Whirlpool and the Queenston. In this case, a rectangular model boundary was used, with dimensions similar to the radial mesh. The mesh, however, is constrained by joint elements spaced 0.2 m apart. In any case, the zones gradually begin to increase in size away from the excavation surface (Fig. 10). The two-dimensional models use an interior load reduction to simulate the three-dimensional excavation process. For the three-dimensional models the

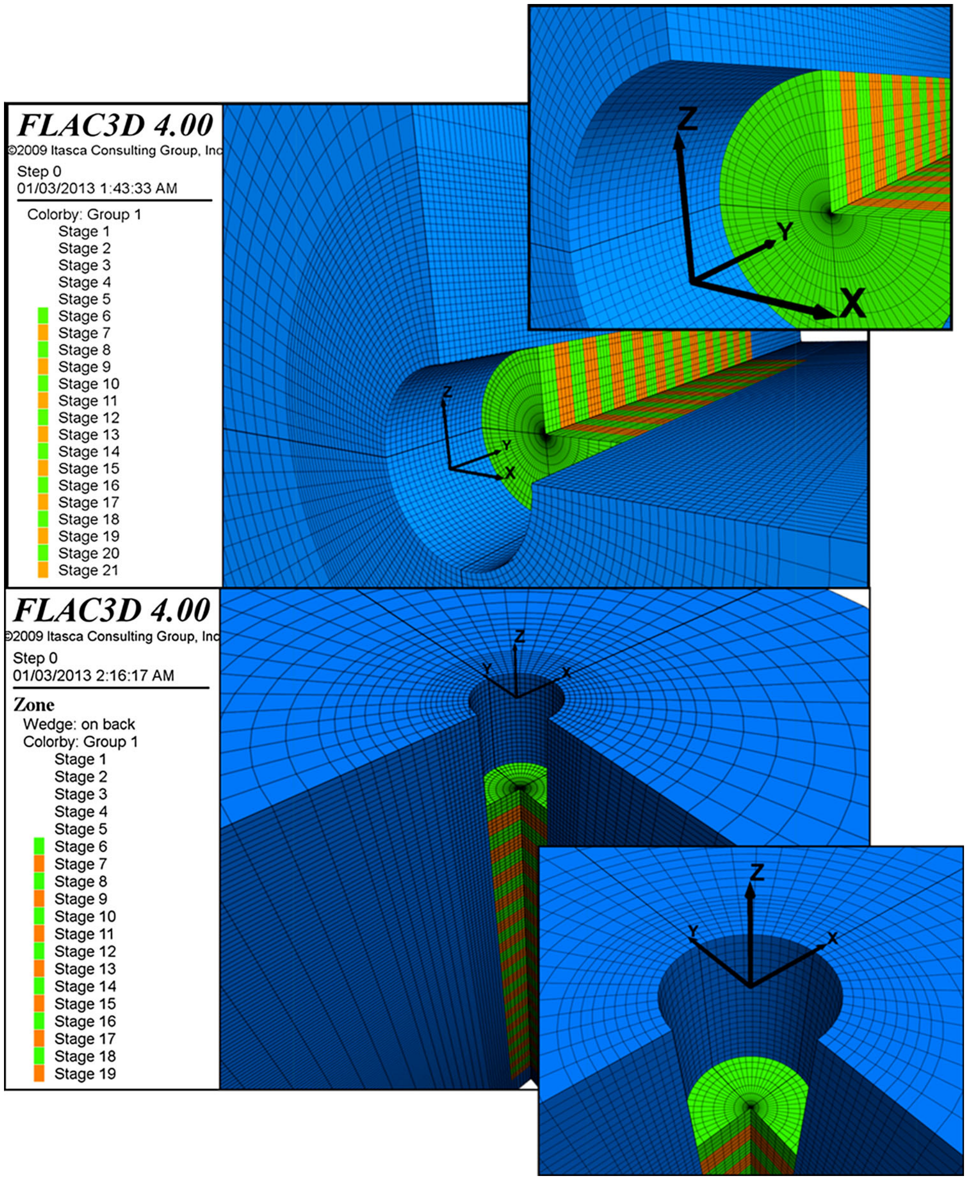

Fig. 10 Mesh setup for the NTP (*top*) and the DGR (*bottom*) showing zone dimensions (see *insets* for detail) increasing away from the excavation surface. The axes arms are 5.0 m

tunnel excavation was completed in 2 m stages over a length of 75 m.

A similar setup was used for the DGR models (Fig. 10). The zones at the excavation surface of the DGR shaft models have lengths of 0.06 and 0.45 m for the two- and three-dimensional models, respectively.

4.3 Rock Support Considerations

Overbreak measurements from the NTP show that once the tunnel had passed under St. Davids Buried Gorge and into the high regional stress field, the depth of the overbreak was typically greater than 2 m. The depth increased to the order of 4 m around a chainage of 3 + 500 m and reportedly reached a maximum of 6 m beyond 3 + 500 m. A gap of roughly 6 m between the face and the point of the primary rock support installation forced the removal of the yielded rock mass prior to the installation of bolts and steel channels. The notch dimensions were measured prior to support installation and minimal visible deformation was observable after support was installed. Forward spiles were used to bridge the gap to minimize the volume of overbreak being removed from the tunnel crown. In areas where spiles were not installed, the notch could fully develop representing the unsupported rock mass behaviour, which allows for back calculation.

An example of the typical notch that formed when spiles were not installed is shown in Fig. 11, and measures 3.78 m deep. Because the notch was fully formed prior to the installation of the rock support, when spiles were not

Fig. 11 Typical overbreak notch at the Niagara Tunnel Project encountered in the high horizontal stress zone, Zone 4 from Fig. 2b

installed, the numerical simulation of the rock support has been neglected. Thus, the numerical results should yield the maximum notch geometries.

5 Model Results

The NTP provides an opportunity to back analyse the numerical stress and strength scenarios that most closely match the measured overbreak and chord closure measurements. The comparison between DISL and the LAM models is used to demonstrate the need to capture the anisotropic strength and stiffness to correctly capture both the overbreak dimensions and the chord closure measurements. In two dimensions, the influence of horizontal lamination cannot be captured for the DGR site models because the lamination plane is in the same plane as the numerical model. In this case, the DISL and UBJT DY models are compared.

5.1 Back Analysis of the NTP

The observed depth of the overbreak from Fig. 11 was used as a target to determine the starting stress state for the analysis using the empirical relationship of Martin et al. (1999), which was modified to include CI for brittle spall modelling by Diederichs (2007).

The DISL or the similar cohesion weakening friction hardening modelling approaches have been shown to be very effective in capturing the correct notch geometry associated with brittle rock mass failure (Diederichs 2007; Hajiabdolmajid et al. 2002; Hajiabdolmajid 2001).

Back analysis was conducted at three different tunnel chainages; 3 + 000, 3 + 250, and 3 + 500. These chainages were selected because the overbreak depth changed from 2 to 4 m over this 500 m section of the tunnel. The back analysis modelling was conducted in stages, with a layer of complexity added at each stage to narrow down the range of inputs that correctly capture the overbreak and chord closure measurements. The stages that were used are as follows:

(a) DISL models with mean properties over a wide range of stress scenarios
(b) DISL models with ±1 standard deviation of the mean properties
(c) DISL models including dilation
(d) LAM models with mean properties over a narrowed stress scenario range
(e) LAM models with varying joint element properties
(f) UBJT DY models with mean properties

The starting K_o ratio was determined using the mean empirical depth of the relationship presented by Diederichs (2007):

$$\frac{r}{R} = 0.5\left(\frac{\sigma_{max}}{CI} + 1\right) \tag{4}$$

where r is the maximum depth of the notch, R is the radius of the excavation, and $\sigma_{\max}$ is the maximum tangential stress at the excavation boundary calculated by $3\sigma_1 – \sigma_3$. The maximum tangential stress for the NTP models was determined using $\sigma_{max} = 3\sigma_{\mathrm{H}} – \sigma_{\mathrm{v}}$. Substituting this into Eq. 4 and solving for σ_{H} results in:

$$\sigma_{\mathrm{H}} = \frac{\sigma_{\mathrm{v}} + \mathrm{CI}\left(2\frac{r}{R} - 1\right)}{3} \tag{5}$$

Using this equation and an assumed vertical stress gradient of 0.026 MPa/m, 140 m depth, a target depth of failure of 4 m (chainage 3 + 500 m), tunnel radius of 7.2 m, CI of 15 MPa and solving for σ_{H}, the maximum horizontal stress would be 11 MPa. This results in a K_o ratio of 3.4. For simplicity, 3.5 was used as the starting point.

Perras et al. (2014) found that the typical 4 m notch geometry could be captured using the mean rock properties and a K_o of 4 using the DISL approach. However, using these same values and changing the elevation of the model sections does not adequately capture the measured depth of the overbreak. To capture the changing overbreak depth at different chainages, the stress field was modified, and the mean rock properties were adjusted by ± 1 standard deviation.

Diederichs (2007) stated that the DISL method on its own does not adequately capture displacements, but dilation should be used to induce reasonable displacements. Generally, a higher dilation angle allows for a greater post-yield volumetric expansion of the rock mass. This results in increased strains, over zero dilation models, around the modelled excavation in the plastic yield zone and can be

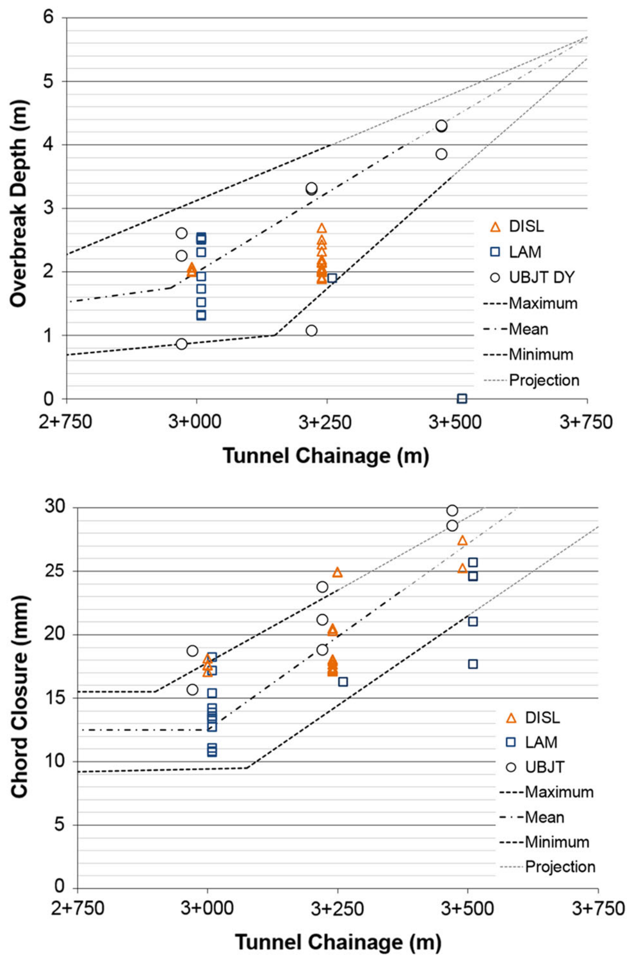

Fig. 12 DISL, LAM, and UBJT DY model results in comparison to the measured **a** overbreak and **b** chord closure from the NTP (limits from Perras et al. 2014) with inset model examples. Note that an offset in the chainage was used to more clearly plot the results

used to correctly capture the strains and displacements. Vermeer and de Borst (1984) recommended using a dilation angle, Ψ, which was smaller than the friction angle, ϕ. Hoek and Brown (1997) stated that values for Ψ are typically around $\phi/8$. These are equivalent to the dilation parameter m_d and m_r, respectively. Walton and Diederichs (in press) suggested estimating the appropriate constant dilation angle using Eq. 6:

$$\frac{\Psi}{\phi} = 0.5\left(\frac{\mathrm{CI}}{\sigma_{\max}}\right) - 0.1 \tag{6}$$

The results of the two-dimensional DISL models are plotted against the measured overbreak and chord closure limits in Fig. 12a and b, respectively. Due to the constraint of the TBM head, chord closure measurements at the NTP could only begin to be measured approximately 6–7 m back from the face. To correct the closure measurement limits the elastic convergence, u_{ie}, can be estimated using Eq. 7;

$$u_{ie} = \frac{R(1+v)}{E}(p_o - p_i) \tag{7}$$

where R is the tunnel radius, v is Poisson's ratio, E is Young's Modulus, p_o is the hydrostatic in situ stress, and p_i is the internal support pressure. If the average Young's Modulus and Poisson's ratio (0.35) are used with the stress at 140 m depth in Eq. 7, the resulting elastic convergence is 14 mm including convergence in front of the face.

According to Vlachopoulos and Diederichs (2009) the Longitudinal Displacement Profile, using a plastic radius of 11 m, would predict 25 % of the maximum displacement to occur at the face. Yield at the face was not a common occurrence at the NTP. Therefore, a conservative estimated correction of 25 % of the elastic convergence or 3.5 mm has been applied to the limits of Fig. 12b.

A variety of stress and strength inputs can yield overbreak dimensions, estimated from the maximum yield strain contour of 0.001, within the limits of the measured values from the NTP. To narrow the stress and strength scenario which yields the measured overbreak dimensions, at each chainage, dilation was used to increase the numerical chord closure to match the measured in situ values. The results include models with a dilation of 0 and those with a range of dilation parameters between 0.1 and 6.0. Figure 12b shows that chord closures from the DISL numerical results could only be captured at chainages of 3 + 250 and 3 + 500 m within the observed limits. At a chainage of 3 + 000 m, the minimum achievable chord closure is shown in Fig. 12b. In fact, when the dilation parameter is used, the chord closure first decreases as the dilation parameter is increased. However, a minimum chord closure is reached, and further increases in the dilation parameter increase the numerical chord closure again (Fig. 13). Using dilation also increases the overbreak depth above the value of the same model without dilation. For the example shown in Fig. 13, the models with dilation show only a marginal increase in the overbreak (0.1–0.2 m) over the model without dilation.

Because the DISL approach with different dilation values is unable to produce chord closures below a certain level, the LAM modelling approach was employed to control the lateral closure using the lamination properties. The LAM approach gives overbreak depth results similar to the DISL approach and can correctly capture the overbreak geometry (notch shape) within the measured limits (Fig. 12a). The inclusion of the laminations induces anisotropic stiffness in the model, which is controlled by the joint element properties, as previously discussed.

The normal (K_N) and shear (K_S) stiffnesses of the intact bedding in a rock mass are difficult to measure accurately in the laboratory and are seldom reported in the literature.

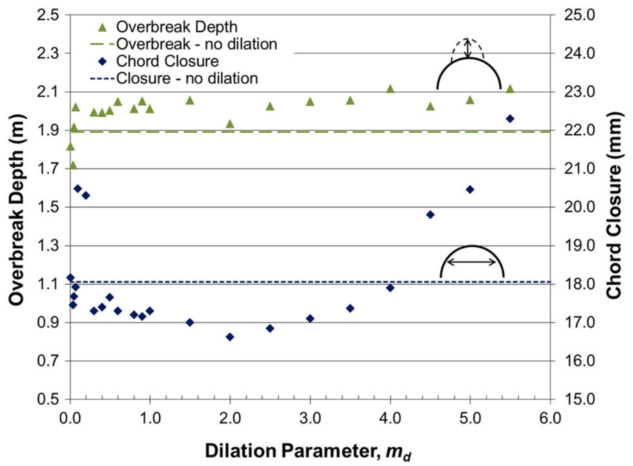

Fig. 13 Influence of the dilation parameter on the overbreak depth and chord closure determined from a DISL model at a tunnel chainage of 3 + 250 m using the +1 standard deviation properties and a $K_o = 3$ and a $K_{Hh} = 1$

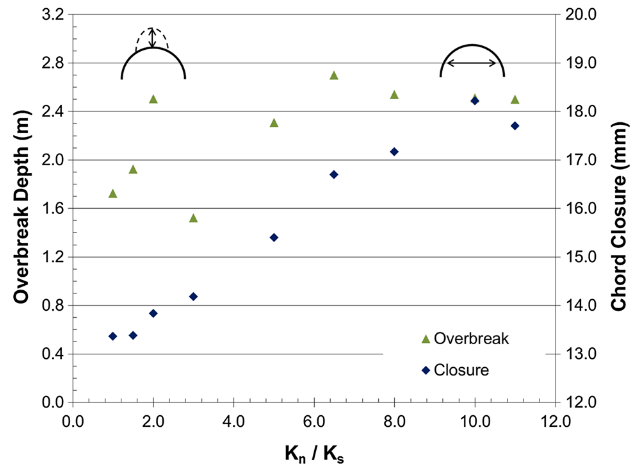

Fig. 14 Influence of the joint stiffness ratio, K_n/K_s, on the overbreak depth and chord closure determined from a LAM model at a tunnel chainage of 3 + 000 m using the +1 standard deviation properties and a $K_o = 2.5$ and a $K_{Hh} = 1.5$

Savilahti et al. (1990) reported that for intact rock $K_N = K_S$, and Barton (2007) stated that for very good joint surfaces, K_N/K_S should be between 11 and 15. For the modelling presented in this paper, K_N/K_S ratios between 1 and 11 were evaluated because the bedding planes were intact. The shear stiffness was calculated using this range of ratios after the normal stiffness was determined using Eq. 3.

Figure 14 shows the relationships between the stiffness ratio (K_N/K_S) and the overbreak depth and chord closure results from an example model at a chainage of 3 + 000 m, with mean rock properties and stress ratios of $K_o = 2.5$ and $K_{Hh} = 1.5$. The models demonstrate that there is a direct relationship between the stiffness ratio and the chord closure. As the stiffness ratio is decreased, the chord closure also decreases.

There is a less clear relationship between the overbreak depth and the stiffness ratio, although generally the overbreak depth increases with increases in the stiffness ratio. The more erratic relationship is due, in part, to stress channelling, which has been described in more detail by Perras (2009). The stress is channelled through the beams above the crown of the excavation, and each consecutive beam above the crown can build stress before completely yielding, including the failure of the joint element, which sheds the stress to the beam above. This creates a non-linear relation: as K_S is reduced, there is an increase in the horizontal displacement, which causes more convergence into the excavation (Perras 2009).

The target chord closure at a chainage of 3 + 000 m has a range of 6–14 mm, and the target overbreak range is 0.9–3.2 m. The model results shown in Fig. 14 indicate that a stiffness ratio of less than three is needed to achieve the targeted chord closure and overbreak depth. The laminations in the model helped to capture both the chord closure and overbreak targets.

However, the horizontal nature of the laminations in the Queenston Formation means that two-dimensional models can only capture this behaviour when a horizontal tunnel is modelled. For a vertical shaft, a three dimensional model is required to incorporate the anisotropic behaviour. As discussed previously, this has been done using the UBJT DY approach, which was first applied to the NTP to determine if it matched the results of the DISL and LAM approaches.

The range of overbreak depths is illustrated in Fig. 15 from the modelled results for the NTP. The maximum shear strain contours are shown on the left, with the plastic yielding on the right. The maximum shear strain contours give a more representative shape to the notch geometry, and visible damage can be expected to occur within the continuous zone of contours that intersect the excavation surface.

Utilizing the maximum shear strain contour approach, the model that most closely represents the NTP notch is shown in Fig. 15 (middle). The depth of the notch in the model is 3.85 m, and it is roughly 7.0 m wide at the tunnel crown, measured horizontally, similar to that observed at around 3 + 500 m (Fig. 11). The UBJT DY model has been shown to capture the behaviour for the NTP, and it incorporates ubiquitous joints that can capture the strength anisotropy of the Queenston Formation.

5.2 Rock Mass Anisotropy and Excavation Orientation

As previously mentioned, to model the DGR shaft in the horizontally laminated Queenston Formation and

Fig. 15 Comparison of maximum shear strain (*left*) and plastic yield (*right*) for the range of stress conditions modelled. $K_o = 3$ (*top*), $K_o = 4$ (*middle*) and $K_o = 5$ (*bottom*)

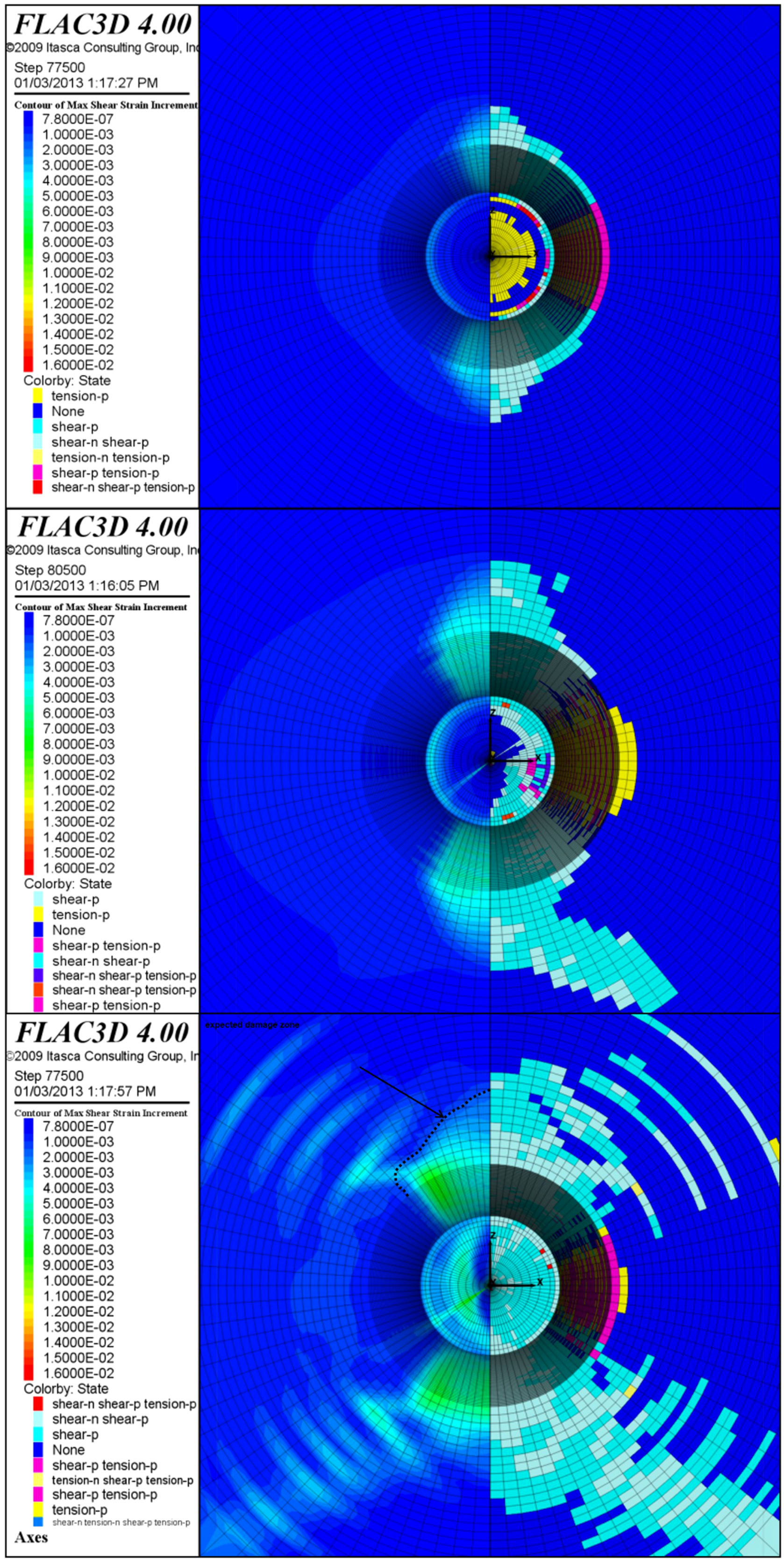

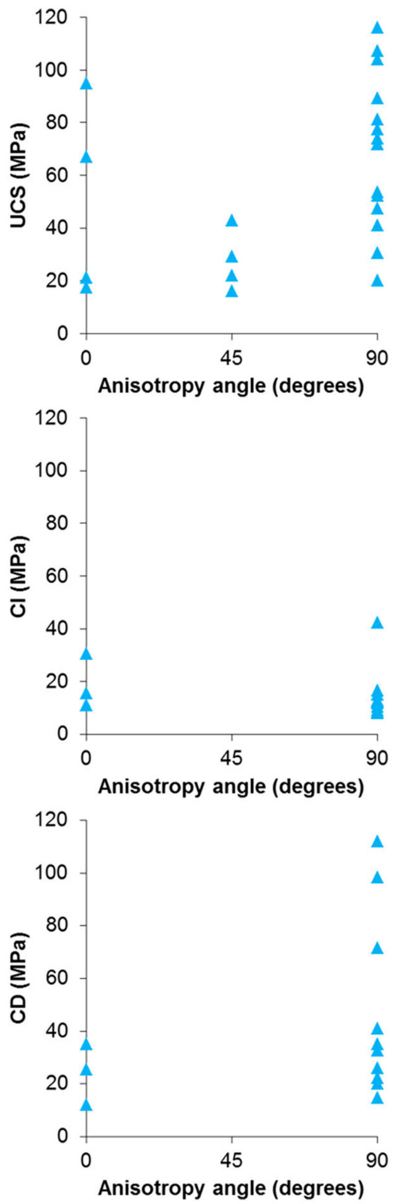

Fig. 16 UCS, CI and CD thresholds estimated by the strain method versus lamination angle for the Queenston Formation (modified from Ghazvinian et al. 2013)

incorporate the anisotropic strength, the UBJT DY approach has been applied. However, the appropriate properties for the rock mass should first be discussed.

As expected, the Queenston behaves in the typical anisotropic manner, with minimum strength values when the bedding is inclined at 45° to the loading axis, as shown in Fig. 16. CD likely follows the same trend, although there were no stress–strain curves for the 45° samples available. The CI thresholds, however, are similar at both 0° and 90° and are in fact roughly in the same range as the peak strength of the 45° samples. If this behaviour at the laboratory scale is applied conceptually to the rock mass strength envelope, then the orientation of the excavation with respect to the orientation of the bedding planes changes the observed behaviour, as conceptually illustrated in Fig. 17.

A UCS test with horizontal bedding should reflect the strength of the sidewall in a horizontal excavation with σ_1 orientated parallel to the horizontal bedding. Similarly, a UCS test with vertical bedding should reflect the strength of the crown and invert in a horizontal excavation with σ_1 orientated parallel to the horizontal bedding. In a horizontal excavation in a rock mass with horizontal bedding, the beds in the crown and invert are able to deflect and fail into the excavation. Micro-cracks should propagate more easily along the bedding than across it.

Conceptually (Fig. 17), this means that for a horizontal tunnel in horizontal bedding and high horizontal stress CD = CI, and the rock mass will behave in a brittle fashion. For a vertical shaft in a rock mass with horizontal bedding, the beds are unable to deflect into the excavation, and this confinement allows for friction to be mobilized on the bedding planes if yielding occurs, which conceptually means CD > CI (Fig. 17). The rock mass, therefore, would behave as a shearing rock mass. In addition, because a cross section through the vertical shaft in the rock mass with horizontal bedding would be parallel to the plane of anisotropy, the stress flow around the excavation is unaffected by the bedding in the plane of interest (Fig. 17 inset shaft illustration). In this case, there should be no advantage in modelling the anisotropic stiffness with a three-dimensional model. The stress flow around a horizontal tunnel is influenced by the anisotropic rock mass (Fig. 17 inset tunnel illustration) and the behaviour of a model with isotropic properties versus anisotropic properties gives different results, as discussed in more detail by Perras (2009). The orientation of the plane of anisotropy and the stress field is an important consideration and will be discussed in more detail in Sect. 6.0.

5.3 Forward Prediction of the DGR Shaft

Numerical modelling of the shaft through the Queenston Formation was conducted by NWMO (2011) using a variety of methods. The depth of the EDZ from NWMO's study (2011) had a range of 2.03–3.42 m, as shown in Fig. 18. The lower end of the range was predicted using the DISL approach, and the upper end was predicted using a strain weakening approach. Experience from the NTP would suggest that the behaviour at the tunnel was brittle in nature.

In this study, two-dimensional modelling of the DGR shaft was also conducted using the DISL approach and the three rock mass property sets from Table 2. At the DGR site, the dimensions of the EDZ are of interest because of

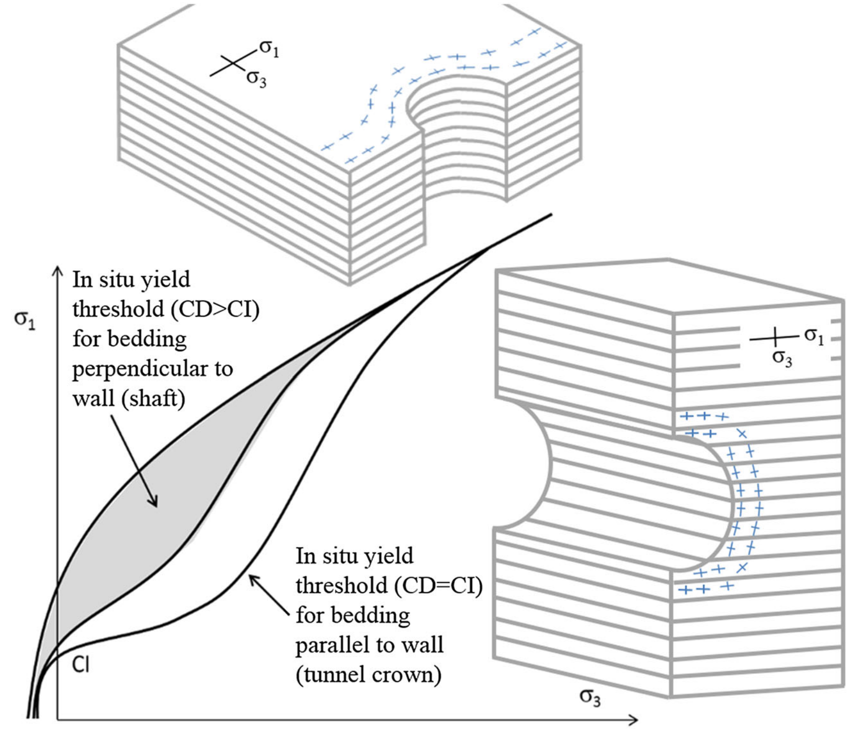

Fig. 17 Interpretation of the DISL model combined with post CI interaction with bedding weakness planes in a tunnel and shaft including illustrations of stress field trajectories around each type of excavation

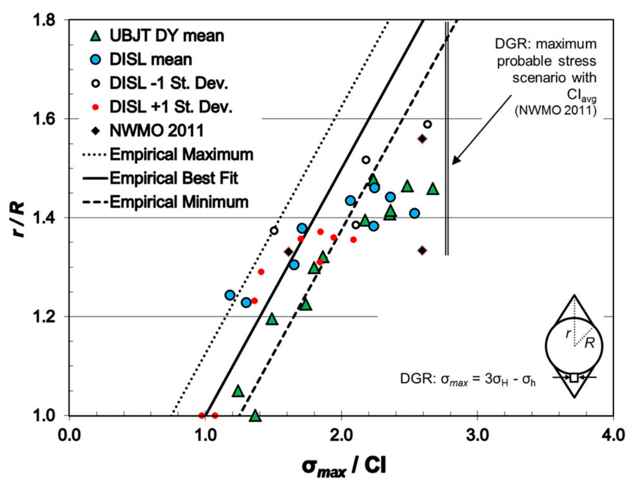

Fig. 18 Maximum depth of plastic yield for sites. *Solid* and *dotted lines* are average, maximum and minimum spalling limits, respectively, based on Martin (1997) and Diederichs (2007)

the potential flow path through this zone of damage. Engineered cut-off structures must be designed to intersect the EDZ to minimize the flow along the potential pathway.

To determine the range of the expected depth of damage, the stress ratios K_o and K_{Hh} were varied such that the normalized tangential wall stress (σ_{max}/CI) range fell between 1.0 and 2.7. Below a normalized-tangential wall stress of one, there should be negligible damage around the excavation (i.e. isolated micro-cracking only), and the upper limit of 2.7 represents the maximum value based on the probable stress scenario at the DGR site within the Queenston Formation using the average CI (NWMO 2011).

The DISL results from this study are bracketed by the results presented by NWMO (2011), as shown in Fig. 18. Even when using the −1 standard deviation properties, the results from this study are only approximately 0.15 m deeper than the maximum predicted depth of damage from the NWMO (2011) study. As expected, generally the models with high strength (+1 standard deviation) had lower depths of damage than the weaker models tested.

However, a consistent non-linear relationship between σ_{max}/CI and the depth of damage is demonstrated (Fig. 18). When the σ_{max}/CI ratio is greater than two, the linear empirical limits tend to overestimate the depth of damage, when compared to all the numerical results.

Examining the UBJT DY results shows that when σ_{max}/CI is smaller than two, the model predicts less damage than the equivalent DISL model. Above this level, there is good agreement with the DISL model results. This suggests that the failure mechanism in the DGR case can be adequately captured with an isotropic continuum approach, and that the ubiquitous joints have minimal influence because of their orientation relative to the excavation.

Three examples are presented in Fig. 19, which show the maximum shear strain contours and plastic yield around the excavation models. The top model shows variable plastic yield along the shaft. The plastic yield is associated with the staging of the excavation and the corner of the

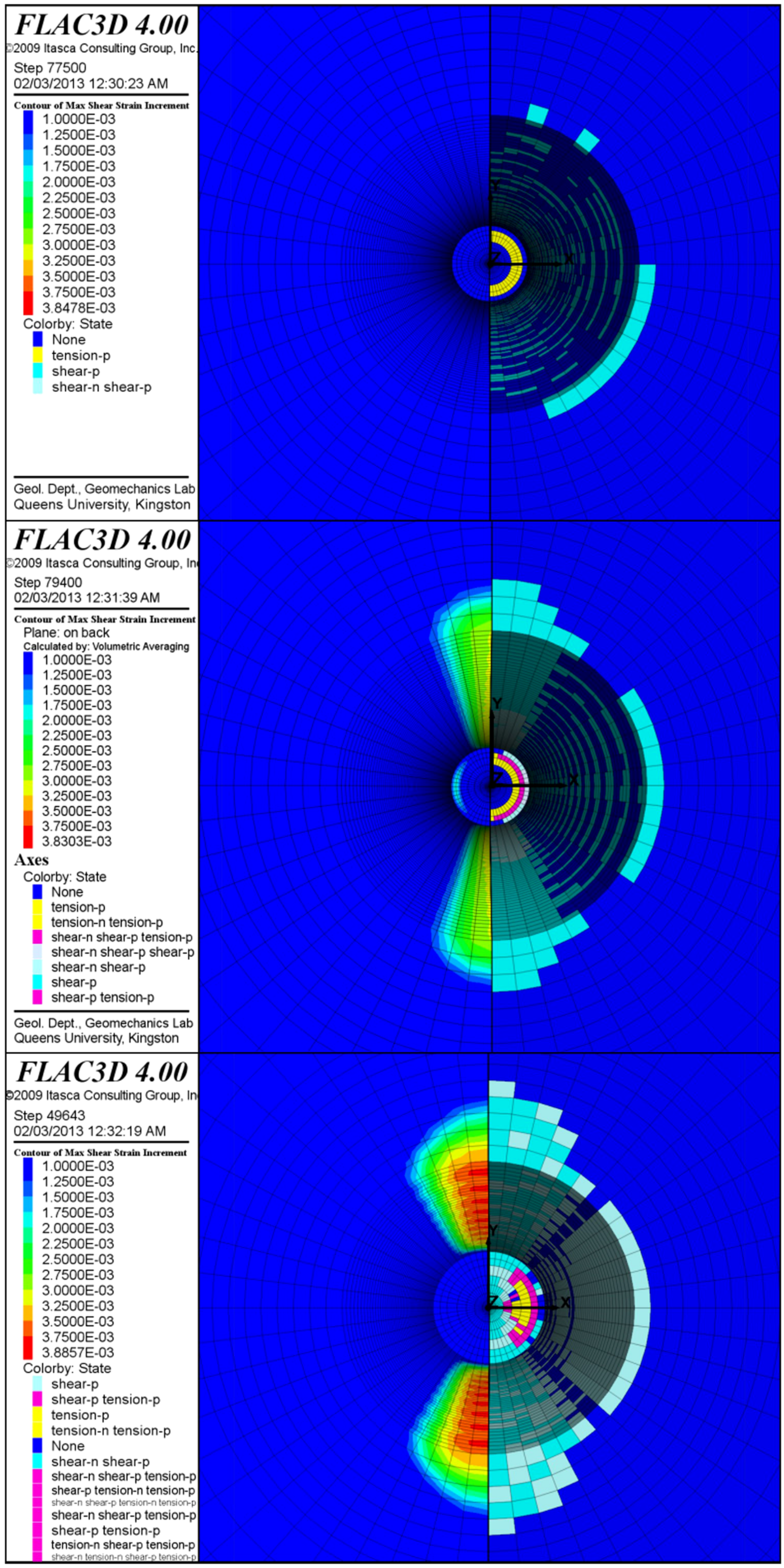

Fig. 19 Maximum shear strain (*left*) and plastic yield (*right*) for the minimum (*top*), intermediate (*middle*) and maximum (*bottom*) stress scenarios for the DGR shaft

sidewall with the face. The average maximum depth was taken from the analysis.

The middle and bottom models in Fig. 19 represent the intermediate and maximum stress scenarios, respectively. The latter shows a maximum depth of damage of roughly 2 m. Figure 19 also demonstrates that the shape of the damaged zone is different than that predicted by the NTP models. The notch is more rounded and wider in comparison to the NTP models. This is the result of the gravitational influence at the NTP and the larger stress ratio in the plane perpendicular to the excavation orientation.

For the NTP, the in-plane stress ratio is K_o, with a maximum value of approximately 5.0, whereas at the DGR, it is K_{Hh}, with a maximum value of approximately 3.2. The possibility of a notch developing decreases as the in-plane stress ratio decreases. This is an important aspect to consider for such cases where cut-offs are required to minimize the flow of radionuclides through the EDZi.

6 Discussion

The notch at the NTP was influenced by the requirements to remove loose rock above the TBM shield prior to the installation of the rock support. Intense scaling was conducted and as each damaged bedding slab was removed during the scaling operations, the small amount of confinement provided by the damaged bedding slab was also removed. This allowed the damage to propagate deeper into the rock mass as scaling continued. In the case of the NTP, the process was assisted by gravity, but it was initiated by the horizontal stresses concentrated at the crown in relation to the sub-horizontal bedding orientation.

Numerically, the plastic yield limit marks the maximum extent of micro-cracking. The density of micro-cracking increases towards the excavation boundary with the micro-cracks being isolated away from the excavation boundary and becoming interconnected closer to excavation boundary producing macro-cracks. In practice, when rock support is installed close to the face, the overbreak can be considered to be the limit of macro-cracking. However, with intense scaling or an unsupported span the overbreak can extend beyond the macro-cracked region. A methodology described by Perras et al. (2012) to determine the excavation damage zones from continuum models, demonstrated that the volumetric strain could be used to distinguish between different types of excavation damage, micro- and macro-cracks. Numerically the micro-cracked area is defined as plastic yielding with volumetric contraction (EDZo), meaning that the micro-cracks are unable to propagate to become interconnected because the confinement is causing contraction. The macro-cracked area is defined with volumetric extension (EDZi) and low confinement, meaning that the micro-cracks can propagate and coalesce into macro-cracks and with low confinement can become open flow pathways at the excavation surface (HDZ).

The occurrence of the transition from volumetric extension strain to contraction for a tunnel and shaft model is illustrated in Fig. 20. The maximum shear strain is plotted on the left, and the volumetric strain contours are plotted on the right. Within the zone of damage, there are both positive and negative volumetric strains. In the logic of FLAC3D, the contraction is negative, and the extension is positive (Itasca 2009). It can be seen in Fig. 20 that the switch from contraction to extension occurs within the notch (within the zone of shear strain) for both the tunnel and the shaft. However, there is a much smaller difference in the depths of the extension-contract transition and the shear strain increment (0.001) for the shaft model than the tunnel.

It should be noted that it is not the reversal point of the gradient, but in fact the sign change that marks the beginning of extension because there is an elastic volumetric strain that has to be overcome before extension can occur, as discussed by Perras et al. (2012). The EDZi at the NTP would be predicted numerically to be 1.5 m; however, as a result of the scaling and the near horizontal bedding parallel to the maximum stress, the overbreak propagated to the extent of the micro-cracking (EDZo), roughly 4 m in the calibrated model. Thus, in a shaft scenario, the overbreak should be less than the EDZo because the orientation of the bedding with respect to the stress field results in a more isotropic behaviour (Fig. 17 inset) and gravity does not influence the damaged rock mass in the same manner as it does in a tunnel excavation. This is further illustrated in Fig. 20, where the tunnel model shows a larger difference between the extent of shear strain (EDZo) and the extension-contraction transition (EDZi limit) than the shaft model.

To determine the relationship between the different modelling approaches for the NTP in a manner similar to that for the DGR (Fig. 18), the results are normalized and plotted in Fig. 21. In this figure, the model results that conformed to the measured overbreak depth and chord closure are plotted. For the case of the NTP, the UBJT DY model results show the highest sustained stresses that yield overbreak depths in the maximum target ranges. However, using joint properties with 80 % of the rock mass strength, overestimated the chord closure when the mean rock mass properties were used, and underestimated it when the +1 standard deviation properties were used.

The LAM models are also able to capture both the maximum overbreak depth ranges and the chord closure, however, only at reduced confining stresses over the UBJT DY models. None of the models were able to correctly

Fig. 20 Maximum shear strain (*left*) and volumetric strain (*right*) for the NTP model with $K_o = 4$ and $K_{Hh} = 1.4$ (*top*), the best fit UBJT DY model, and for the DGR model with $K_o = 1.6$ and $K_{Hh} = 3.2$ (*bottom*), which represents the maximum depth from the DGR models. The axis is 4.05 m in length

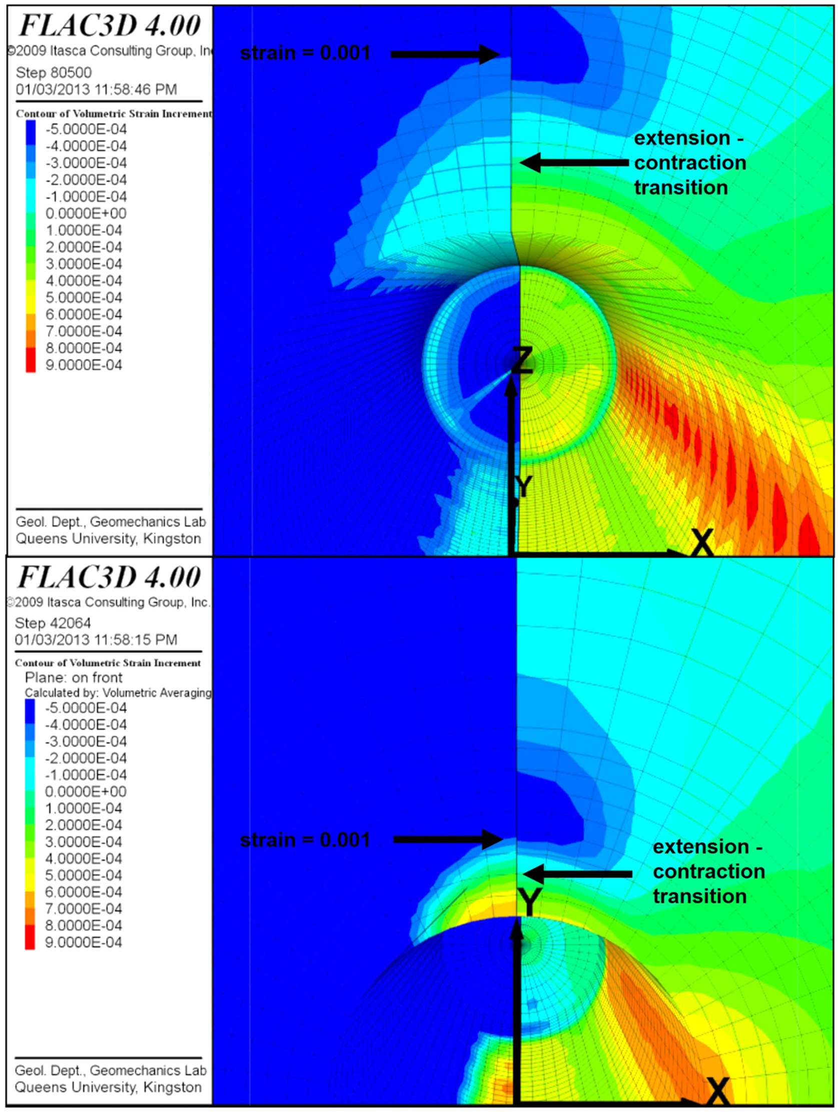

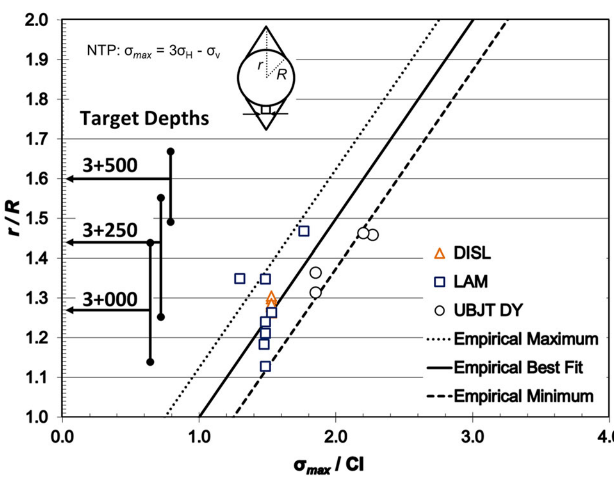

Fig. 21 Normalized tangential wall stress versus overbreak depth for the numerical models that matched the measured overbreak and closure measurements

capture both the overbreak depth and chord closure at chainage 3 + 500 m. It was possible to capture one or the other using the variations in the properties. It is possible that the majority of the overbreak at 3 + 500 m should be close to 4 m in depth, and that, on occasion; depths of 6 m may have been encountered as a result of other geological structures or by excessive scaling.

The plastic yield and maximum shear strain contours show the typical notch-shaped geometry observed in other excavations in brittle rocks, such as at the underground research laboratory (URL) operated by Atomic Energy of Canada Ltd. (AECL) for example (Martin 1997). As the stress ratio increases, the plastic yield zone becomes less of a notch and 'stringers' of plastic yielding begin to occur when the stress ratio increases beyond the slope of the Mohr–Coulomb failure envelope in the σ_1–σ_3 space. These 'stringers' are in fact realistic damage that represents

Table 3 Final ranges of stress ratios and property sets at the three chainages modelled which gave rise to overbreak depths and chord closures within the measured limits

3 + 000 m			3 + 250 m			3 + 500 m		
K_o	K_{Hh}	Properties	K_o	K_{Hh}	Properties	K_o	K_{Hh}	Properties
2.5–4.0	1.2–1.5	+1 Sd Dev.	3.5 2.9–3.6	1.2 1.0–1.8	Mean +1 Sd Dev.	3.2	1.25	Mean

isolated micro-cracks that do not coalesce into visible damage because they remain in a confined state in the rock mass. This has been demonstrated at AECL's URL by monitoring the micro-seismic activity in front of an excavation face (Martin 1997).

The target mean normalized damage radii, r/R, are indicated for the different chainages in Fig. 21, and it can be seen that the empirical limits underestimate the required normalized wall stress predicted by the models, similar to the DGR models. The DISL and LAM model results in Fig. 21 were able to capture both the overbreak and chord closure limits that were measured at each chainage. The UBJT DY models were unable to capture both target measurements.

The corresponding ranges of stresses and properties that result in overbreak and closure results similar to those measured at the NTP are shown in Table 3. By matching both the overbreak depth and chord closure measurements with the numerical results there is increased confidence, over only match one criteria, that a unique solution has been determined. These results generally indicated that the K_o ratio increases with depth, and the strength also increases with depth, which is consistent with the measurements presented earlier (Figs. 5, 6).

The in situ variability of the strength, stiffness, and stress and the installation of rock support during excavation accounts for the range of the measured overbreak depths and chord closure values, as reported by Perras et al. (2014).

The rock support would only have a small influence on the depth of yielding because of the delay in installation. However, the yielded material is retained, and the true depth of yielding is un-measureable. Confinement is provided by the rock support and could be sufficient to suppress further propagation of the notch when it is beyond EDZo in situ.

This study was aimed at a back analysis of the NTP overbreak and closure. The different modelling approaches were calibrated to the measurements from the project. The understanding gained from this back analysis was applied to the DGR site to investigate the performance of the shaft in this formation at a deeper level but with a much less severe stress ratio between any of the principal stresses.

7 Conclusions

The back analysis of the NTP showed the importance of incorporating the anisotropic stiffness and strength because the LAM modelling approach was the most successful at capturing the measured overbreak depth and chord closure measurements from the site. All three modelling methods were able to capture the measured overbreak geometry or chord closure. However, the maximum projected targeted values at a chainage of 3 + 500 m could not be captured using the same model properties. Individually, the overbreak geometry or the chord closure measurements could be captured with all the modelling approaches. For the models that captured both target values, a narrower range of K_o, K_{Hh}, and rock properties at the specific chainages was determined over the general ranges stated for the whole project.

A similar methodology was implemented to predict the depth of damage around the DGR shaft in the Queenston Formation. The results were in agreement with those of previous studies. All of the modelling methods gave similar depths of damage above a σ_{max}/CI value of two. Below this threshold, conservative maximum damage depths were predicted using the DISL approach. The maximum depth of damage was determined to be 1.92 m, using the −1 standard deviation properties. For the modelled cases, the average depth of damage was determined to be 1.0 m. The explicit incorporation of anisotropic stiffness in the DGR models could lead to decreased damage depth prediction. The modelling showed that the observed normalized depth of failure at the NTP would over-predict the depth of damage expected in the Queenston Formation at the DGR site.

Acknowledgments The authors would like to thank the Nuclear Waste Management Organization of Canada (NWMO) and the National Science and Engineering Research Council of Canada for supporting this research financially. The discussions with the NWMO staff and their comments regarding this topic are also greatly appreciated. Ontario Power Generation kindly provided the Niagara Tunnel Project data to the authors for previous research, and the continued use of the data is greatly appreciated.

References

Amann F, Button EA, Evans KF, Gischig VS, Blumel M (2011) Experimental study of the brittle behaviour of clay shale in rapid

unconfined compression. Rock Mech Rock Eng 44:415–430. doi:10.1007/s00603-011-0156-3
Armstrong DK, Carter TR (2006) An updated guide to the subsurface Paleozoic stratigraphy of southern Ontario. Ont Geol Surv Open File Rep 6191:214
Armstrong DK, Carter TR (2010) The subsurface Paleozoic stratigraphy of southern Ontario. Ont Geol Surv (Special Vol. 7)
Barla G, Bonini M, Semeraro M (2011) Analysis of the behaviour of a yield-control support system in squeezing rock. Tunn Undergr Sp Technol 26:146–154. doi:10.1016/j.tust.2010.08.001
Barton N (2007) Rock quality, seismic velocity, attenuation and anisotropy. Taylor and Francis Group, New York, p 720
Bergstrom SM, Kleffner M, Schmitz B, Cramer BD (2011) Revision of the position of the Ordovician-Silurian boundary in southern Ontario: regional chronostratigraphic implications of 13C chemostratigraphy of the Manitoulin Formation and associated strata. Can J Earth Sci 48:1447–1470. doi:10.1139/E11-039
Brady BHG, Brown ET (2006) Rock Mechanics for underground mining, 3rd edn. Springer, Dordrecht, The Netherlands
Brogly PJ, Martini IP, Middleton GV (1998) The Queenston Formation: shale dominated, mixed terrigenous-carbonate deposits of Upper Ordovician, semi-arid, muddy shores in Ontario, Canada. Can J Earth Sci 35:702–719. doi:10.1139/e98-021
Delmar R, Charalmbu H, Gschnitzer E, Everdell R (2006) The Niagara Tunnel Project–an overview. Tunn Association of Can Conference, Niagara Falls, Canada
Diederichs MS (2003) Rock fracture and collapse under low confinement conditions. Rock Mech Rock Eng 36(5):339–381. doi:10.1007/s00603-003-0015-y
Diederichs MS (2007) The 2003 Canadian geotechnical colloquium: mechanistic interpretation and practical application of damage and spalling prediction criteria for deep tunnelling. Can Geotech J 44:1082–1116. doi:10.1139/T07-033
Diederichs MS, Martin CD (2010) Measurement of spalling parameters from laboratory testing. In: Proceedings of Eurock, Lausanne, Switzerland
Fortsakis P, Nikas K, Marinos V, Marinos P (2012) Anisotropic behaviour of stratified rock masses in tunnelling. Eng Geol 141–142:74–83. doi:10.1016/j.enggeo.2012.05.001
Ghazvinian E, Perras M, Diederichs M, Labrie D (2013) The effect of anisotropy on crack damage thresholds in brittle rocks. In: Proceedings ARMA 2013, San Francisco, CA, USA
Gorski B, Anderson T, Conlon B (2009) DGR site characterization documents, technical reports TR-07-03 and TR-08-11. www.nwmo.ca. Accessed 24 Mar 2014
Gorski B, Anderson T, Conlon B (2010) DGR site characterization documents, technical reports TR-08-24 and TR-08-36. www.nwmo.ca. Accessed 21 Feb 2014
Gorski B, Rodgers D, Conlon B (2011) DGR site characterization document, technical report TR-09-07. www.nwmo.ca. Accessed 10 Nov 2011
Gross MR, Fischer MP, Engelder T, Greenfield RJ (1995) Factors controlling joint spacing in interbedded sedimentary rocks: integrating numerical models with field observations from the Monterey Formation, USA. Geol Society, Lond, Spec Publications 92:215–233. doi:10.1144/GSL.SP.1995.092.01.12
Gschnitzer E, Goliasch (2009) TBM modification for challenging rock conditions—a progress report of the Niagara Tunnel Project (NTP). Geomech Tunn 2(2):168–178. doi:10.1002/geot.2009000016
Haimson BC (1983) SAB-Niagara GS No. 3 hydrofracturing stress measurements and permeability tests in holes NF-3 and NF-4. Ontario Hydro Report: 85357
Hajiabdolmajid VR (2001) Mobilization of strength in brittle failure of rock. PhD thesis, Queen's University, Kingston, Ontario, Canada
Hajiabdolmajid V, Kaiser PK, Martin CD (2002) Modelling brittle failure of rock. Int J Rock Mech Min Sci 39:731–741. doi:10.1016/S1365-1609(02)00051-5
Hoek E, Brown T (1997) Practical estimates of rock mass strength. J Rock Mech Min Sci 34(8):1165–1186
Hoek E, Carranza-Torres C, Corkum B (2002) Hoek–Brown failure criterion–2002 edition. In: Proceedings of ARMS-TAC Joint Conference, Toronto, Canada. www.rocscience.com. Accessed 22 Apr 2014
Intera Engineering Ltd. (2011) Descriptive Geosphere Site Model. NWMO Tech. Report, DGR-TR-2011-24
Itasca (2009) FLAC3D: Fast Lagrangian analysis of continua in 3 dimensions. Software User's Manual. Itasca Consulting Group Inc., Minneapolis, Minnesota, USA
Lo KY, Lee YN (1990) Time-dependent deformation behaviour of Queenston shale. Can Geotech J 27:461–471. doi:10.1139/t90-061
Martin CD (1997) Seventeenth Canadian Geotechnical Colloquium: the effect of cohesion loss and stress path on brittle rock strength. Can Geotech J 34:698–725. doi:10.1139/t97-030
Martin CD, Kaiser PK, McCreath DR (1999) Hoek-Brown parameters for predicting the depth of brittle failure around tunnels. Can Geotech J 36:136–151. doi:10.1139/t98-072
Novakowski KS, Lapcevic PA (1988) Regional hydrogeology of the Silurian and Ordovician sedimentary rock underlying Niagara Falls, Ontario, Canada. J Hydrology 104:211–236. doi:10.1016/0022-1694(88)90166-7
NWMO (2011) Geosynthesis. NWMO Technical Report, DGR-TR-2011-11
Perras MA (2009) Tunnelling in horizontally laminated ground: the influence of lamination thickness on anisotropic behaviour and practical observations from the Niagara Tunnel Project. M.Sc.Eng. thesis, Queen's University, Kingston, ON
Perras MA, Diederichs MS (2014) A review of the tensile strength of rock: concept and testing. Geotech Geol Eng 32:525–546. doi:10.1007/s10706-014-9732-0
Perras MA, Langford C, Ghazvinian E, Diederichs MS (2012) Important rock properties for numerical modelling of underground excavations. In: Proceedings of Eurock 2012, Stockholm, Sweden
Perras MA, Ghazvinian E, Diederichs MS, Lam T (2013) Queenston Formation: tunnel back analysis and forward shaft prediction. In: Proceedings of the 47th US Rock Mechanics/Geomechanics Symposium, San Francisco, CA, USA
Perras MA, Diederichs MS, Besaw B (2014) Geological and geotechnical observations from the Niagara Tunnel Project. Submitt Bull Eng Geol Environ. doi:10.1007/s10064-014-0633-5 (Online first article)
Read RS, Chandler NA, Dzik EJ (1998) In situ strength criteria for tunnel design n highly-stressed rock masses. Int J Rock Mech Min Sci 35(3):261–278. doi:10.1016/S0148-9062(97)00302-1
Russell DJ (1981) Controls on shale durability: the response of two Ordovician shales in the slake durability test. Can Geotech J 19:1–13. doi:10.1139/t82-001
Sandford BV (1961) Subsurface stratigraphy of Ordovician rocks in southwestern Ontario, Geological Survey of Canada, Paper 60–26
Savilahti T, Nordlund E, Stephansson O (1990) Shear box testing and modelling of joint bridges. In: Barton N, Stephansson OAA (Ed) Proceedings of the International Symposium on Rock Joints, Loen, Norway. Balkema, Rotterdam, pp295–300
Sloss LL (1953) The significance of evaporates. J Sediment Res 23(3):143–161. doi:10.1306/D42695F3-2B26-11D7-8648000102C1865D
Stearn CW, Carroll RL, Clark TH (eds) (1979) Geological Evolution of North America. John Wiley and Sons, Toronto

Tamulonis K, Jordan T (2009) Examination of the Queenston Delta in central New York for geological carbon dioxide storage. AAPG Search and Discovery Article #90090, AAPG Annual Convention and Exhibition, Denver, Colorado, June 2009

Vermeer PA, de Borst R (1984) Non-associated plasticity for soils, concrete, and rock. Heron 29(3):1–64

Vlachopoulos N, Diederichs MS (2009) Improved longitudinal displacement profiles for convergence confinement analysis of deep tunnels. Rock Mech Rock Eng 42:131–146. doi:10.1007/s00603-009-0176-4

Walton G, Diederichs MS (in press) Dilation and post-peak behaviour in plasticity models for tunnelling applications

Winder CG, Sanford BV (1972) Stratigraphy and paleontology of the Paleozoic rocks of southern Ontario. 24th International Geological Congress, Montreal, Quebec, excursion A45–C45, p73